Mineral Concentration of Amino Acids on the Early Earth: Aspartate - Layered Double Hydroxide Minerals

Brian Grégoire[a#], Valentina Erastova[b#], Dawn L. Geatches[c], Stewart J. Clark[d], H. Christopher Greenwell[b*], Donald G. Fraser[a].

[a]Department of Earth Sciences, University of Oxford, South Parks Road, Oxford, OX1 3AN, UK

[b]Department of Earth Sciences, Durham University, South Road, Durham, DH1 3LE, UK

[c] Daresbury Laboratory (STFC), Warrington, WA4 4AD, UK

[d]Department of Physics, Durham University, South Road, Durham, DH1 3LE, UK

[#]co-first authors

* Corresponding author: E-mail: chris.greenwell@durham.ac.uk

Abstract

The role of mineral surfaces in concentrating and facilitating the polymerisation of simple protobiomolecules during the Hadean and Archean has been the subject of much research in order to constrain the conditions that may have led to the origin of life on early Earth. Here we examine the adsorption of the amino acid aspartate on layered double hydroxide minerals, and use a combined computer simulation – experimental spectroscopy approach to gain insight into the resulting structures of the host-aspartate material. We show that the uptake of aspartate occurs in alkaline solution by anion exchange of the dianion form of aspartate, rather than by surface adsorption. Anion exchange only occurs at values of pH where a significant population of aspartate has the amino group deprotonated, and is then highly efficient up to the mineral anion exchange capacity.

1. Introduction

Since Bernal first suggested some seventy years ago that minerals such as aluminosilicate clays could have played an important role in the origin of life (Bernal, 1949), a wide range of experiments has been undertaken to understand the structure and reactivity of simple protobiomolecules and biomolecules at mineral surfaces (Hazen and Sverjensky, 2010), and whether permutations of minerals, reaction conditions and environments could constrain the search for the origin of life on Earth (Mejias *et al*., 1999). Assuming that a legacy of those original biomolecules remains within cellular make up, and that once evolved, the main functional units of information transfer were determined, the search for the origin of life on Earth has centred around the formation of either the first nucleic acid sequences (Powner *et al*., 2009) or the first proteins (Rode 1999).

Recent work shows that nucleic acid precursors, lipids and amino acids can all be plausibly created on an early Earth (Patel *et al*., 2015), and the RNA World has proved to be a resilient hypothesis for the journey from geochemistry to biochemistry (Gilbert, 1986; Hernandez and Piccirilli, 2013). On the other hand the presence of all known biogenic amino acids in meteorites, as well as the ready availability of amino acids via abiotic Strecker and Miller-Urey synthesis, suggests the "protein first" scenario is also a relevant and plausible alternative hypothesis (Fitz *et al*., 2007) and the abiotic generation of oligopeptides is of importance, in any case. With the presence of the amino acid building blocks on the early Earth and elsewhere seemingly indisputable, the generation of peptides requires a process of concentration and subsequent condensation to form peptide bonds and this has been studied by numerous researchers over the years, see (Lambert, 2008) for a recent review.

An elegant route for achieving amino acid concentration and peptide bond formation has been via dense salt brines, used as experimental analogues for early Earth marine evaporites. In brines, peptide-forming dehydration reactions occur naturally. Once the

concentration of sodium ions becomes high enough, their inner hydration spheres are lost. The enthalpy of re-hydration of the sodium is then favourable enough to drive peptide bond formation via a condensation reaction to re-establish the sodium hydration sphere. This is named the salt induced peptide formation (SIPF) reaction (Schwendinger and Rode, 1992). The addition of trace copper (II) ions to the brine leads to a preferential chelation configuration by two amino acids and, hence, regio-selectivity in subsequent peptide forming reactions (Plankensteiner *et al*., 2004). Other studies have probed the role of heterogeneous catalysts, especially those plausible on the early Earth. Notably, the possible roles of mineral surfaces in protecting, selecting, concentrating, templating and catalysing reactions of prebiotic organic molecules are recurrent themes in discussions of life's origins. The adsorption of amino acids has been studied on a variety of minerals, including alumina (Basiuk and Sainz-Rojas, 2001), silica (Bujdák and Rode, 1997; Martra *et al*., 2014) and aluminosilicate cationic clays (Bujdak *et al*., 1994; Fraser *et al*., 2011; Fraser *et al*., 2011). Some of these studies have also been undertaken on specific chiral surfaces of minerals in order to shed light on both the polymerisation of amino acids, and the origin of homochirality (Hashizume *et al*., 2002). Layered minerals, such as clay minerals, are advantageous for adsorption of protobiomolecules owing to their high surface area, permanent charge and ion exchange capability, and the protecting environment between each 2-dimensional layer.

Layered double hydroxides (LDHs) form a class of naturally occurring and synthetic anionic clays, with the most important group of these materials described by the general formula $[M^{II}_{1-x}M^{III}_{x}(OH)_2]$ $(A^{n-})_{x/n}.mH_2O$, where M^{II} and M^{III} are di- and trivalent cations of similar radii, respectively, A^{n-} is an exchangeable interlayer anion with charge n, and x represents the $M^{II}/(M^{III}+M^{II})$ mole fraction (**see Figure 1**). Owing to their readily varied compositions, anion-exchange properties, surface area and acid/base nature, these materials

74 are attractive for a wide range of materials science applications (Duan and Evans, 2006;
75 Grégoire *et al*., 2012).

76 In previous work, amino acid-intercalated LDH systems have been prepared either by
77 direct co-precipitation of the mineral in the presence of amino acids, or via a reconstruction
78 route, where a mixed metal oxide precursor is rehydrated in the presence of the amino acid
79 (Fudala *et al*., 1999; Pálinkó, 2006; Whilton *et al*., 1997). However in the context of prebiotic
80 chemistry, the ability of an inorganic LDH to exchange a more labile simple inorganic anion,
81 for example chloride or sulphate, with an organic anion such as an amino acid (**see Figure 1**),
82 would have been key to concentrating biomolecules from dilute solutions and it is this
83 exchange that is the subject of the present paper.

84 It has been suggested that large quantities of mixed valence iron LDH minerals were
85 the precursors of banded iron formations (Lascelles, 2007) and, as such, the role of these
86 materials in concentrating biomolecules could have been significant. Other than in the
87 seminal work of Arrhenius and co-workers (Arrhenius, 2003; Kuma *et al*., 1989), few papers
88 have looked at the role of anion exchange in layered double hydroxides in the context of
89 prebiotic chemistry. As with vermiculite gels (Fraser *et al*. 2011), the nano-sized interlayer
90 domain of LDHs provides a "nanoreactor" for confining reactants in a preferred orientation,
91 controlling the regio- and stereo-selectivity of products. Hybrid LDH materials with
92 intercalated amino acids or peptides have been explored for a variety of applications. For
93 example, Hibino investigated the delamination behaviour of LDH sheets for use in polymer
94 composites as a function of the nature of the intercalated amino acids (Hibino, 2004), while
95 Chen *et al*. studied the kinetics of oxidation of cysteine in a restricted environment provided
96 by the interlayer domain of LDH (Chen *et al*., 2009). Demonstrating the added stability of
97 intercalated biomolecules, Wei *et al*. found intercalation of enantio-pure L-Tyrosine

prevented racemisation occurring when the materials were exposed to sunlight, or high temperature (Wei *et al*., 2005).

Despite their utility, LDH and other layered minerals present a challenge to structural analysis, because the interlayer domain is dynamic at room temperature and hydrated at atmospheric humidity, and the materials invariably have long-range order only in terms of the stacking of the layers. Computational chemistry methods have become an essential adjunct to experimental techniques for probing the structure and dynamics of intercalated molecules in layered minerals (Newman et al., 1998). A number of studies of hydrated intercalated layered minerals have been performed using molecular dynamics (MD), including, for example, the interactions of mono-, di- and trivalent carboxylate anions, including amino acids within LDH interlayers (Greenwell *et al*., 2006; Kalinichev *et al*., 2010; Kumar *et al*., 2006; Kumar *et al*., 2007; Pisson *et al*., 2011). These studies have highlighted the differences in interlayer water interactions with inorganic and organic anions. Computational quantum mechanics studies can provide detailed information about specific molecular interactions in mineral interlayer environments (Aimoz *et al*., 2012; Boulet *et al*., 2006). Quantum chemistry methods have also been used to study reactivity of peptides at mineral surfaces (Rimola *et al*., 2007), and this area has recently been reviewed by Coveney *et al*.(Coveney *et al*., 2012).

In order that studies are relevant to the origin of life, realistic geochemical constraints must be set. Since the discovery of the Lost City hydrothermal field (LCHF), the idea that life originates in alkaline media has emerged (Baross and Hoffman, 1985; Kelley *et al*., 2001; Martin *et al*., 2008). In these low temperature hydrothermal vents, reactions between seawater and upper mantle peridotite produce methane and hydrogen-rich fluids that are highly alkaline (pH 9 to 11). Hanczyc *et al*. demonstrated that physicochemical forces that are present in the LCHF can drive the formation of vesicles and their division, strengthening the theory that early life may have been cellular (Hanczyc *et al*., 2003). Alkaline fluids also have many other

123 advantages; they favour phosphate and amine chemistry, and promote acid-base reactions,
124 suitable for the formation of amino acids and a rich library of organic compounds (Ferris and
125 Hagan Jr, 1984; Russell, 2003). From a mineralogical point of view, brucite ($Mg(OH)_2$),
126 formed during the convective hydration of rocks is expected to have existed on the early
127 ocean floor (Schoonen *et al*., 2004) and may have been abundant. The structure of LDHs
128 derives directly from the brucite structure, and may result from weathering of Mg-rich and
129 Al-rich minerals, and also from the formation of mixed valent Fe-rich minerals.

130 The nature of the interlayer anion in the LDH structure is also an important
131 consideration. Owing to its symmetry and charge density, the carbonate anion is
132 thermodynamically preferred and its presence in the interlayer domain prevents further anion
133 exchange. In Archean sea water, atmospheric CO_2 and magmatic sources both contributed to
134 the presence of carbonate species (predominantly bicarbonate or dissolved CO_2). In alkaline
135 hydrothermal fluids, despite the elevated pH, the carbonate alkalinity is less than one third of
136 sea water values because of the absence of a magmatic source (Kelley *et al*., 2005). The
137 elevated concentration of calcium further contributes to the removal of free carbonate anions
138 from water, evidenced by the high quantity of calcite/aragonite minerals found at such
139 locations resulting in carbonate chimneys 30 to 60 meters tall (Kelley *et al*., 2001; Kelley *et*
140 *al*., 2005; Lang *et al*., 2010; Martin *et al*., 2008). The salinity of the early ocean is believed to
141 have been 1.5 or 2 times that of today's ocean (Sleep, 2010), and therefore, chloride anions
142 are likely to have been the most prevalent in the formation and stabilisation of LDH minerals
143 near such hydrothermal fields. In the present study, we use experimental conditions indicative
144 of these. The adsorption isotherms were carried out in the pH range of the hydrothermal field
145 (pH 9 and 11) where we hypothesise LDH minerals may have been present in sufficient
146 quantity to have played a significant role in the concentration of amino acids. Alkaline pH

147 further favours the presence of anionic amino acids with a deprotonated carboxylate group
148 and deprotonated amino group suitable for their intercalation in the LDH galleries.

149 The present study brings together experimental methods and computational modelling
150 to examine the exchange of aspartate (Asp) with chloride (Cl^-) within LDHs, and characterise
151 the resultant organo-minerals. Aspartate was selected for this study because of its anionic
152 nature due to its carboxylate side chain, and because it has been identified as one of the earlier
153 amino acids to have been incorporated into biochemistry (Engel and Nagy, 1982; Hall *et al*.,
154 1971). By varying the pH of the external solution over a range of alkalinity, geochemical
155 constraints can be placed on the exchange of amino acids, such as aspartate, into the mineral
156 interlayer. Such alkaline conditions are considered to have been geochemically relevant at
157 low temperature hydrothermal seeps (Baross and Hoffman, 1985). Importantly, the minerals
158 used are redox-stable structural analogues of the green rust Fe(II)/Fe(III) LDHs thought to
159 have been prevalent on the Archean Earth (Arrhenius, 2003).
160

161 ## 2. Synthesis and Intercalation Methodology

162 Though it is possible to prepare Mg_RAl-Cl (see definition below) LDHs directly via co-
163 precipitation chemistry under an inert gas to prevent carbonate inclusion, it was decided to
164 prepare Mg_RAl-CO_3 LDHs, and then exchange the carbonate for chloride using the procedure
165 of Iyi *et al*. (Iyi *et al*., 2011). This is more relevant to early Earth chemistry and delivers more
166 uniform, larger crystal sizes than direct synthesis of the chloride containing LDH, thus
167 facilitating reproducible adsorption isotherm measurements. All chemicals ($MgCl_2.6H_2O$,
168 $AlCl_3.6H_2O$, 1M HCl solution, L-Aspartic acid, absolute ethanol, (ACS reagent grade) were
169 provided by Sigma Aldrich and were used as supplied.

170 As this work includes materials with different composition, the following
171 nomenclature was used through this manuscript. Mg_RAl-X refers to LDH materials composed

of Mg and Al cations whose proportions are expressed by the value, R = n(Mg)/n(Al). X represents the interlayer anions, namely, CO_3^{2-}, Cl^- or $Asp^{-/2-}$ (for aspartate) in this study. If the R value or X is not explicitly stated, we refer to generic LDH materials with any R value or X anions.

2.1. Chloride-layered double hydroxide preparation

A 0.4 M solution of $MgCl_2$ and $AlCl_3$ salts dissolved in water, with Mg:Al = 2:1 or 3:1, was added slowly (0.3 mL/min) to a solution of Na_2CO_3 (0.25 M). The pH was kept at 11 by simultaneous addition of NaOH (1 M) solution using an auto-titrator (with an error of approximately +/- 0.05 pH units). After complete addition of the cation solution, the slurry was aged for 20 h at 25°C. The final white crystalline solids were washed repeatedly with deionised water and dried at 60°C overnight. The Mg_RAl-CO_3 was converted to Mg_RAl-Cl by an exchange reaction according to the method proposed by Iyi *et al*. (Iyi *et al*., 2011). An ethanolic solution was prepared by diluting a 1 M HCl solution in 5 mL of ethanol. This was slowly added to a vigorously stirred Mg_RAl-CO_3 suspension (0.662 mmol of Mg_RAl-CO_3 i.e. 161.3 mg and 199.9 mg for the ratio R = 2 and 3, respectively) in 45 mL ethanol solution under nitrogen flow. The factor f, defined by Iyi *et al*. as f = [HX] / (2 x $[CO_3^{2-}]$) where [HX] represents the monoprotic acid concentration, was set to 1.5. The suspension was stirred for 1 h at room temperature under N_2. The suspension was filtered with a polycarbonate membrane (0.2 μm), and the solid washed thoroughly with absolute ethanol and dried at 60°C. The elemental composition of these LDH phases is reported in **Table A1 (SI)**.

2.2. Adsorption isotherm experiments

To avoid carbonate contamination, adsorption isotherms were run in a glove box purged by N_2, at 25°C and ultrapure water was boiled, purged with N_2, and allowed to cool down to

197 room temperature. 0.2 mmol of Mg_RAl-Cl (i.e. 48.0 mg and 59.7 mg based on the formula
198 $Mg_2Al(OH)_6(Cl)$, 1.5 H_2O and $Mg_3Al(OH)_8(Cl)$, 1.5H_2O respectively) was added to a
199 racemic solution of aspartic acid, with the aspartic acid concentration varied from 2 to 100
200 mmol/L. The pH was adjusted to either 9 or 11 by addition of a NaOH solution at 1 M. Each
201 experiment was duplicated. To ensure equilibrium had been reached, the suspensions were
202 stirred for 20 h. Finally, the white polycrystalline solid was separated by filtration.
203
204 *2.3 Hydration state dependence of structure*
205 Three relative humidity levels were considered: RH 0%, 25% and 88%. To achieve these, the
206 LDH materials were initially placed for 48 h in an oven at 150°C. The LDH phases were
207 removed from the oven and placed for a further 48 h in a desiccator filled with a 55% w/w
208 solution of sulphuric acid, to produce a relative humidity of 25%, and then for 48 h with a
209 solution of 20% w/w to give a relative humidity of 88%. After each step, the sample weights
210 were measured allowing the determination of the interlayer water content. The formulae of
211 the phases obtained are reported in **Table A6 (SI)**. For given interlayer water content, the
212 samples were analysed by ATR-FTIR and XRD.
213
214 *2.4. Mineral characterisation*
215 *Powder X-ray diffraction (XRD)*. Patterns were recorded with a Phillips X'Pert Pro MPD
216 diffractometer in reflection geometry using Cu $K\alpha_1$ radiation (λ = 1.5406 Å). Samples were
217 finely ground and continuously rotated to improve statistics. The 2θ range was between 5–70°
218 with a step size of 0.01671° and a scan time per step set at 2s giving a scan rate of 2°/min. In
219 order to make the determination of the cell parameters easier, the XRD lines were fitted with
220 Lorentzians. The fitting was made with the minimum number of Lorentzians per XRD peak
221 needed to obtain a regression coefficient better than 0.99.

222 *Fourier Transform Infra-Red (FTIR) Spectroscopy*. FTIR spectra of solution or samples at
223 different relative humidity were acquired on a Varian FTS-7000 spectrometer equipped with a
224 diamond attenuated total reflectance (ATR) cell. A KBr beamsplitter and a deuterated
225 tryglycine sulphate (DTGS) detector were used to perform the analysis. For liquid, a 0.1M
226 aspartate solution was prepared. Intensities were then corrected to reflect the real
227 concentration after dilution with HCl or NaOH to obtain different pH values. Solids were
228 analysed on their own, without any specific preparation. The spectra were acquired with a
229 resolution of 4 cm^{-1} and 100 acquisitions were averaged per sample.
230
231 *Elemental analysis*. The Mg:Al ratio of the synthesised and exchanged LDH was determined
232 by inductive coupled plasma - atomic emission spectrometry (ICP-AES) on an Ultima
233 apparatus (Jobin Yvon). Prior to measurement, the LDH materials were dissolved in a 2 M
234 HNO_3 solution and the solution filtered before analysis.
235
236 *2.5. Adsorption isotherm analysis*
237 After the LDH mineral had been in contact with the aspartate solution for 20 h, the amino acid
238 solution was filtered and analysed by high performance liquid chromatography (HPLC) to
239 quantify the amount of amino acid adsorbed. A chiral column was used to measure the L to D
240 aspartate isomer ratio in solution to study any enantioselectivity. The stock aspartate solutions
241 served as standards. All runs were made in duplicate and three analyses per run were
242 averaged. Two µl of the sample were injected into a Phenomenex Chirex 3126 (D)-
243 penicillamine LC column (150 x 4.6 mm), equipped with a 15 mm guard column. Analysis
244 was performed in the isocratic mode with a mobile phase consisting of 85% of a 2 mM $CuCl_2$
245 solution and 15% of methanol, pumped at 1 ml/min. The calculated separation factor, α, using

these conditions is 1.42. The limit of detection based on this method was calculated from the regression curve and was found to be 1.06 mmol/L.

3. Computational Simulation Methodology

To investigate the structure and properties of the interlayer region in more detail we have used a combination of quantum mechanical, periodic, density functional theory (DFT) calculations and molecular dynamics (MD) simulations.

3.1. Quantum mechanical calculations

Model structures of the Mg_RAl-Asp systems were constructed and the energy of each model was iteratively minimised through adjustment of its atomic coordinates and calculating the total energy using DFT. As DFT is computationally demanding, and the intercalated LDH models were relatively large (between 150 to 400 atoms) and lacking in symmetry that would otherwise speed-up such calculations (by enabling a reduction in the number of k-points used to sample the Brillouin zone, for example) the total number of models investigated was constrained to those described as follows.

3.1.1. Model Construction

The initial structures were based on the magnesium hydroxide ($Mg(OH)_2$) mineral brucite. LDH models were created with the formulae $[Mg_2Al(OH)_6]^+$ and $[Mg_3Al(OH)_8]^+$, respectively. Each model contained two interlayer regions, with enough aspartate amino acids to balance the layer charge. Each periodic model contained two interlayer's (**see Figure A1, SI**) and all simulation cell angles and lengths were free to vary.

Aspartate Models. Within the simulations, pH was taken into account by changing the protonation state, and thus charge, on the aspartate, -1was applied for aspartate at pH below the pKa of the amine group (pKa = 9.6) and -2 for pH higher than the pKa of the amine group.

Mg_2Al LDH Models. Supercells were prepared with formulae $[Mg_{24}Al_{12}(OH)_{72}].(^-O_2CCHNH_2CH_2CO_2^-)_6$ and $[Mg_{24}Al_{12}(OH)_{72}].(HO_2CCHNH_2CH_2CO_2^-)_{12}$. All aspartates were initially orientated with the long axes, defined as being between the two carboxylate groups, perpendicular to the LDH layers (as shown in **Figure A1a, SI**). The model containing the aspartates with charge -1 reached a plateau in its geometrical minimisation, and had difficulty in achieving atomic force convergence at lower than 0.05 eV/Å. This indicated that the force convergence criteria imposed on it were artificially too tight. The total energy of this model was converged to 10^{-5} eV, matching the total energy convergence of all other models and therefore the results are comparable.

Mg_3Al LDH Models. The supercell had a formula of $[Mg_{24}Al_8(OH)_{64}].(^-O_2CCHNH_2CH_2CO_2^-)_4$. A number of aspartate starting configurations were assembled in order to reduce the possible configurational bias, which is larger at lower LDH charge density owing to there being more space per amino acid to sample (**see Table A2**, **SI**).

Hydration states. To investigate the effect of intercalated water on the geometry of the interlayer, aspartate models were set up with: no water, two waters per aspartate and five waters per aspartate. The water molecules were placed with an approximately uniform spread around the aspartates without a pre-defined orientation (**Table A2, SI** collates the full information of the model set up, including the labelling of the models that will be used from this point onwards).

3.1.2 Density Functional Theory Simulation Methodology

DFT calculations were carried out using CASTEP (Clark *et al*., 2005), a plane-wave pseudopotential DFT code. Plane-waves are particularly suited as the basis set for periodic models.

Choice of pseudopotential. The pseudopotentials represent the ion-electron interactions, and their choice depends on a number of factors, for example, accurate, simulated spectroscopy demands pseudopotentials with 'hard' cores (Martin, 2004), whereas structural relaxations are equally amenable to 'hard' or 'soft' i.e. ultrasoft pseudopotentials. Both types of pseudopotentials were employed in the study, norm-conserving for the LDH with R = 2 (Lee, 1996), and ultrasoft (Vanderbilt, 1990) for the LDH with R = 3. Also, one system ($[Mg_2Al(OH)_6]^+0.5Asp\ -2.H_2O$) was simulated with both potentials to assess the effect of pseudopotential type. The pseudopotential determines the size of the basis set required for the expansion of the valence electron wavefunctions; these were represented by 550 eV for the LDH with R = 2 and 380 eV for the LDH with R = 3, both of which achieved energy convergence tolerances to better than 1 meV per atom. The Brillouin zone integrations (commonly known as k-point sampling) were performed on variously sized Monkhorst-Pack grids (Monkhorst and Pack, 1976), according to the size of the models. All geometries (except for Mg_2Al containing aspartates of charge -1) achieved the same force tolerance criteria of 0.03 eV/Å.

Choice of functional. The exchange and correlation effects were treated with the generalised gradient approximation (GGA) of Perdew Burke and Ernzerhof (PBE) (Perdew *et al*., 1996), as this is more suitable for molecular bonding than the local density approximation.

Optimisation method. The electronic energy was minimised using density mixing and the total atomic energy using the Broyden-Fletcher-Goldfarb-Shanno (BFGS) algorithm (Head and Zerner, 1985), based on the reduction of forces acting on the nuclei, under which all unit cells and all ions were allowed to relax to their geometrical equilibria. In a study by Ugliengo *et al*. it was demonstrated that inclusion of dispersive forces was important when studying LDH materials (Ugliengo *et al*., 2009). Van der Waals forces were applied via the DFT semi-empirical dispersion interaction correction (DFT-SEDC) (McNellis *et al*., 2009), specifically Grimme 06 (Grimme, 2006). The following convergence criteria were used for all models (unless otherwise stated): electronic energy: 1×10^{-7} eV; total energy: 1×10^{-5} eV/ion, and all calculations were non-spin polarised.

3.1.3 Density Functional Theory Simulation Analysis

Structural properties. Simulated powder X-ray diffraction patterns (XRD) were created from the equilibrated models using the Reflex module within Materials Studio (Accelrys, 2012). The simulated radiation sources were $Cu_{\alpha 1}$; the diffractometer range was 2θ from 5° to 70°; the temperature factor was atomic and the line shift Bragg-Brentano. Neither asymmetry-correction nor any lattice strain was applied. The simulated structure XRD diffraction patterns, calculated interlayer spacings, and snapshots of the final optimised structures are in the supplementary information (**Table A3** and **Figure A3** to **Figure A14, SI**).

Atomic charge calculations. Following full relaxation of the lattice and ions to the convergence criteria described above, the charge density of the models was analysed using Mulliken population analysis (Mulliken, 1955; Mulliken, 1955; Mulliken, 1955; Mulliken, 1955), which in CASTEP is implemented by first projecting the plane wave states onto a localised basis (Sanchez-Portal *et al*., 1995), followed by analysing these projected states

343 under the Mulliken formalism to produce a population analysis. Mulliken analysis is
344 particularly useful for identifying trends in consistently-parameterised systems (Segall et al.,
345 1996; Segall et al., 1996) rather than for calculating absolute charges due to its sensitivity to
346 the atomic basis set (Davidson and Chakravorty, 1992). The calculated atomic charges were
347 used to adapt the ClayFF force field (Cygan *et al*., 2004) parameters, as described in Section
348 3.2.2 and are given in **Table A4, SI**.
349
350 *3.2 Molecular Dynamics Simulations*
351 To provide further understanding of the structure of the Mg_3Al-Asp LDHs, classical
352 molecular dynamics (MD) simulations were undertaken on these systems, enabling models of
353 greater size, and more representative statistics of the thermally induced dynamics of these
354 systems to be obtained.
355
356 3.2.1. Model construction
357 The model used for MD simulations was based upon the LDH layer coordinates for the
358 Mg_3Al-Asp used in the DFT simulations and is shown in **Figure A2, SI**). The initial step was
359 to create a Mg_3Al LDH surface of 114.56 Å x 110.24 Å. 180 randomly distributed aspartate
360 amino acids, deprotonated at both carboxylic groups (2-) were inserted. The resulting layer
361 was solvated with 20 water molecules per aspartate, totalling 3600 molecules per layer. The
362 layer was replicated 5 times along the crystallographic *c* parameter. Further hydration states
363 were formed through decreasing the number of water molecules, as discussed below.
364
365 3.2.2 Force field selection
366 The ClayFF force field (Cygan *et al*., 2004) was used in this work to model the Mg_3Al-Asp
367 LDH. The charges of the Mg_3Al-Asp LDH were slightly altered from the original ClayFF to

add up to an integer of 1 per unit cell, charges are given in **Table A5 (SI)**. Mulliken charges were assigned from the DFT calculations. Aspartate was modelled with the CHARMM27 force field (MacKerell *et al*., 2000), designed for amino acids and compatible with ClayFF (Underwood *et al*., 2015). Simple point charge (SPC) water was used (Berendsen *et al*., 1981). Both force fields use Lorentz-Berthelot mixing rules for Lennard-Jones interactions.

3.2.3 Molecular Dynamics Simulation Protocol

All molecular dynamics simulations were performed using GROMACS 4.6.2 (Hess *et al*., 2008) software, using a 14 Å cut-off for both Columbic and Lennard-Jones interactions and using periodic boundary conditions in x, y, z directions. After set up the simulation was first energy minimized to remove any high forces. A steepest descent algorithm and force tolerance of 100 kJ/mol/nm per atom was used. MD simulations were run for 1 ns with a 1 fs time-step at a constant temperature of 300 K and a pressure of 1 bar, using the Berendsen thermostat and barostat. Equilibration occurred within the first 100 ps. When the first system with 20 waters per aspartate was equilibrated, 5 water molecules per aspartate were removed, leading to a new model of 15 water molecules per aspartate that was energy minimised again, and equilibrated. By this method a set of simulations with varying degrees of hydration: 20, 15, 10, 7, 5, 3, 2 water molecules per aspartate and a dehydrated system were obtained.

3.2.4 Molecular Dynamics Visualisation and Analysis

All images were produced with VMD 1.9.2 (Humphrey *et al*, 1996). The LDH layer near the bottom/top of the periodic cell was shown on both sides of the visualised cell. The data from the trajectory was extracted with the Tcl (tool command language) scripts in VMD and further analysed with Python 2.7 codes developed by the authors. Graphs were plotted using XMGrace.

4. Results

4.1. Characterisation of Layered Double Hydroxides

The X-ray diffraction patterns of the Mg_RAl-Cl and Mg_RAl-CO_3 LDHs prepared are shown in **Figure 2a** and **2b**. The patterns are characteristic of LDH minerals, with basal reflections observed below 30° 2θ. The Mg_RAl-CO_3 LDH shows characteristic sharp reflections for both R ratios, indicating a crystalline sample with a characteristic interlayer spacing of 7.67 Å and 7.81 Å for the Mg_2Al-CO_3 and Mg_3Al-CO_3 LDH samples respectively, in good agreement with previously reported refined structures for these minerals (Hofmeister and Platen, 1992). The cell *a*-parameter can be used as an indicator of the Mg:Al ratio owing to the difference in ionic radii between Mg and Al, and was found to be 3.044 Å and 3.068 Å for Mg_2Al-X and Mg_3Al-X (X = CO_3 or Cl), in good agreement with literature values (Bellotto *et al.*, 1996; Grégoire *et al.*, 2012; Richardson, 2013) confirming the relative proportions of layer cations reflected the reactants. The Mg:Al ratio determined from ICP-AES agreed well with the quantity of Mg^{2+} and Al^{3+} salt initially added in solution to synthesise the material, and this was not observed to change during subsequent exchange processes. Exchange of carbonate by chloride resulted in expansion of the interlayer space to 7.80 Å and 7.96 Å for the Mg_2Al-Cl and Mg_3Al-Cl samples, respectively, owing to the way that the chloride anion sits between the hydroxide sheets (Hines *et al.*, 2000; Trave *et al.*, 2002). FTIR results show the presence of carbonate vibrational bands at 1365 and 1377 cm^{-1} for Mg_2Al-CO_3 and Mg_3Al-CO_3, respectively. These bands were absent in the FTIR spectra of the Mg_RAl-Cl phases, confirming that the exchange was complete.

4.2. Aspartate Exchange and Adsorption by Chloride Layered Double Hydroxide

Figure 3 shows the adsorption isotherms for exchange of aspartate with chloride in the LDHs. In **Figure 3a**, the Mg_2Al-Cl LDH system shows a typical Langmuir isotherm. After 20 h, a high concentration factor of aspartate is shown even from very dilute solutions (20 mmol/L) to give an interlayer concentration of approximately 7.93 mol/L with a hydration state of 26% H_2O by mass (corresponding to 7 mol H_2O / mol Asp). The Langmuir isotherm reaches a plateau at the maximum anion exchange capacity of 0.5 mol Asp / mol Al, indicating that all chloride has been exchanged and that the intercalated aspartate is all present with a charge of 2-. Further adsorption isotherms were also performed at pH 7 for both LDHs, but no intercalation of amino acid was observed. The adsorption isotherms at pH 9 and 11, displayed in **Figure 3a**, exhibit very similar profiles with a plateau corresponding to the occupation of half of the interlayer sites, presumably because of the preferred intercalation of Asp^{-2} over Asp^{-1}. The adsorption isotherm of Mg_3Al-Cl LDH, displayed in **Figure 3b**, exhibits distinctive features since the maximum of adsorption is reached at a much higher initial solution concentration of aspartate (C_0 = 100 mmol/L).

4.3. Characterisation of the Aspartate Intercalated Layered Double Hydroxide

ATR-FTIR spectra of aspartate solution at different pH were obtained in order to identify the protonation state of the intercalated amino acid as well as the binding conformation of the aspartate molecule (**Figure 4a**). Spectra recorded at pH 7 and pH 9 present very similar features, due to the presence of protonated amino- and deprotonated carboxylate-groups. The large bands at 1587 cm^{-1} and the bands at 1414 (shoulder)/1394 cm^{-1} are attributed to the anti-symmetric stretching and the symmetric stretching of the carboxyl group. The presence of large bands or shoulders may indicate the contribution of the two carboxyl groups and seems to be coupled with the amino bending modes. The band at 1476 cm^{-1} is attributed to the symmetric bending mode of the $-NH_3^+$ moieties. Below 1394 cm^{-1}, modes arise from CH_2

438 (wagging and bending modes) and C-N, C-O and C-C modes (Wolpert and Hellwig, 2006).
439 Distinct changes are observed when the pH is increased to 11. At such a high pH, the
440 aspartate molecules are expected to be fully deprotonated and experimentally, the band at
441 1476 cm^{-1} is observed to disappear completely. Interestingly, the anti-symmetric bands shift
442 to 1557 cm^{-1} and get narrower while the symmetric stretch remains unchanged at 1396 cm^{-1}
443 and becomes more symmetrical. The two carboxyl groups of the molecules are thus no longer
444 distinguishable.

445 Note that the observed FT-IR spectra of intercalated aspartate are very similar to the
446 aqueous aspartate spectra (**Figure 4b**). The carboxyl modes have peaks at 1554 cm^{-1} and
447 1400 cm^{-1}, while the distinct vibrational mode of the $-NH_3$ group expected at 1476 cm^{-1} is
448 completely absent. This suggests that the amino acid is deprotonated. This result is in good
449 agreement with the adsorption isotherm that showed that only half of the interlayer sites to be
450 occupied by amino acids.

451 *4.4. DFT study on Mg_RAl Layered Double Hydroxides*

452 All of the optimised Asp-Mg_RAl model structures and their simulated XRD patterns are in
453 **Figures A3** to **A14, SI**. The interlayer space and the energies of the optimised models are
454 given in the **Table A3, SI**.

455 *4.4.1 Effect of aspartate charge on interlayer structure*.

456 The dependency of the pH (charge of aspartate) on the interaction of aspartate with LDH can
457 be observed. When aspartate is present with -1 charge, a bilayer or mixed/interdigitated
458 bilayer is formed in the interlayer, with a calculated interlayer spacing of 15.54 Å. At higher
459 pH, aspartate carries a 2- charge and, as such, requires fewer molecules to counterbalance the
460 LDH layer charge, in which case the aspartate molecules form a monolayer with an interlayer

461 spacing of 8.27 Å, bridging across the interlayer with opposing carboxylate groups on each
462 amino acid.
463
464 4.4.2 *Effect of hydration state on interlayer structure*
465 Hydration state is variable in layered double hydroxides, depending on the nature of the
466 interlayer, and the ambient humidity. The amount of water in the interlayer region influences
467 the orientation of the other anions present (Newman *et al*., 1998). With the increase of the
468 hydration the increase in the interlayer spacing is observed to change from 3 Å (Mg_2Al) and
469 3.8 Å (Mg_3Al) with no interlayer water, to 4.9 Å (Mg_2Al) and 6.2 Å (Mg_3Al) with 5 waters
470 per aspartate hydration. As the hydration state increases the aspartate molecule rotates from
471 co-planar to the layers to approximately 45° to the layers. When aspartate is co-planar, on
472 some of the aspartates the oxygen atoms on the same carboxylate group bridge to opposite
473 sides of the interlayer, but as hydration increases, the carboxylate groups on each amino acid
474 bind to one layer only, bridging with the second carboxylate group to the other layer. These
475 changes are evident for both Mg_2Al and Mg_3Al systems in **Figure 7**.
476
477 4.4.3. *Effect of initial orientation of aspartate on interlayer configuration*
478 Owing to the confining nature of the interlayer space, the presence of water and the high
479 charge, coupled with strong hydrogen bonding, many local minima on the complex potential
480 energy surface are encountered during optimisation of the LDH structures (Greenwell *et al*.,
481 2006). To counter this, in the present study the effect of the initial molecular arrangement on
482 the final minimised geometry was investigated. An alternative route would be to run an
483 annealing or molecular dynamics run with CASTEP of the models, where thermal motion is
484 applied to the model systems, though these techniques consume large amounts of
485 computational resources.

Four different starting interlayer arrangements of aspartate, with two waters per aspartate were optimised and, in all four cases, the system converged to within very similar energies with the differences circa 0.5×10^{-4} %. In all cases aspartates were observed to lie co-planar, with the long axis parallel to the LDH layers (see **Figures A8 - A11, SI** for the snapshots). The direction of the aspartate in the initial model was not observed to play an important role in the final arrangement. The computationally predicted interlayer spacing ranges from 3.81 Å to 3.95 Å. The small variations of the *d*-spacing between models of the same composition and different initial configurations demonstrates the slight dependence of the final configuration on the starting alignment.

4.5. Molecular Dynamics simulations of the effect of hydration on Layered Double Hydroxide structure.

To complement the experiments and DFT calculations, a variety of different hydration levels of aspartate - Mg_3Al systems were studied with larger-scale MD simulations. We considered hydration levels ranging from from 20 to 0 water molecules per each charge-balancing aspartate. The simulated interlayer structures are displayed in **Figure 8**. Looking at the structures, slight undulations of the hydroxyl layer are observed that are even more prominent at high hydration levels. Such features are often observed in large-scale systems presenting 2-dimensional layers and may result from thermal activation (Thyveetil *et al*., 2007). The basal spacings determined for all the systems are reported in **Table A7 (SI)**. The standard deviation reflects the small fluctuations of the simulation box, as well as undulations of the layer, and allows an estimate of the extent of the undulations as a function of the water content. It can be seen that generally the standard deviation is greater for more hydrated systems, where the layers are more dynamic. This effect most certainly results from the loosening of the electrostatic interactions between the positive layer and the interlayer amino acids, screened

510 by the water molecules. At up to 5 water molecules per aspartate the basal spacing is almost
511 constant, before increasing gradually on further addition of water molecules.

512 In order to investigate the orientation of the amino acid within the interlayer gallery
513 upon hydration, changes of the angle of the vectors assigned between (a) oxygens in sidechain
514 carboxylic groups, (b) oxygens on the back-bone carboxylic groups and (c) between
515 carboxylic carbons, were monitored with respect to the LDH surface (**Figure 9**). For the
516 dehydrated system the vector between oxygen atoms is mainly perpendicular to the LDH,
517 more so than for the carboxylic group of the backbone. While the basal spacing was not
518 observed to change until 3 water molecules per aspartate were added, the sidechain –
519 carboxylate groups underwent more pronounced conformational changes, while the Cα – Cβ
520 backbone orientation remained the same. Obvious changes of the orientation of the sidechain
521 appear over a hydration level of 7 water molecules per aspartate, concomitant with the sudden
522 increase of the basal spacing. The amino acids then attach only with one carboxylate to the
523 surface of the LDH and become more mobile. However, the amino acid never reaches a
524 completely vertical orientation for any hydration content.

525 The analysis of the partial density of the MD simulation boxes allows further insight
526 into the distribution of the water within these phases. As observed in **Figure A15 (SI)**, at up
527 to 5 water molecules per aspartate, the water molecules are located in almost the same plane
528 as that occupied by the aspartate molecules.

529 Further analysis of the dynamics of the system was carried out, looking to pick out the
530 aspartate orientations that could lead to α-peptide (**Figure 10a**) or β-peptide (**Figure 10b**)
531 linkages. In this analysis, the closest carbon in a carboxylic group of a neighbouring molecule
532 within 3.5 Å of a nitrogen atom was found. This means that these pairs can only be included
533 in one of the two peptide-bond formation orientations. In a small number of configurations,
534 two adjacent aspartate molecules may form two β-bonds leading to the formation of cyclic

molecules (**Figure 10c**), such orientations were excluded from the count. **Figure 11** shows the plot of the percentage of the pairs in either α-peptide or β-peptide orientations. Standard deviation on the graph corresponds to the fluctuation in pair numbers through the length of simulation. It is clear from this analysis that, as hydration drops below 7 water molecules per aspartate, amino acids find themselves significantly more likely to form peptide bonds, resulting in a total of 1/3 of all pairs at a reactive distance for 0-3 water molecules per aspartate.

5. Discussion

5.1. Uptake Mechanism of Aspartate by Chloride Layered Double Hydroxide Minerals.

LDH minerals are not stable with respect to dissolution below ~pH 7 and relic deposits of natural LDH minerals on present day Earth are typically associated with alkaline hydrothermal systems. Any LDH minerals formed in this environment would then be stable across the hydrothermal fluid gradient, but susceptible to slow hydrolysis once hydrothermal activity ceased or the mineral deposit exceeded a certain distance from the vent system. On hydrolysis they would have released any concentrated/reacted molecules from within the interlayer. Conceptually, this latter step is critical as once reacted in the interlayer, for oligo- or polypeptides to become functional, they would need to be released, indicating why geochemical gradients are critical to early-Earth proto-biomolecule evolution (Martin and Russell, 2007).

To represent suitable geochemical pH gradients, adsorption isotherms were carried out at pH 7, 9 and 11. The results presented here show that the effect of pH was critical in allowing the successful intercalation and concentration of amino acids in LDHs. At pH 7, all amino acids present in solution have their amino group protonated and exist as zwitterions.

559 Electrostatic repulsion between the positive layer of the LDH and the amino acids in solution
560 prevents either surface adsorption or anion exchange of chloride and no adsorption was
561 observed. Interestingly, in previous work, NMR investigations showed that intercalated
562 glutamate amino acids existed with -1 and -2 charges i.e. with some amino groups protonated
563 (Reinholdt *et al*., 2009). However, in this case, the LDH-amino acid samples were obtained
564 by a co-precipitation route (high pH), whose mechanism of formation differs from the
565 exchange reaction used here, though may be geochemically relevant in some early Earth
566 hydrothermal systems. Similarly, Aisawa *et al*. observed that the intercalation of
567 phenylalanine in a ZnAl LDH by a reconstruction method is preferred at pH 7 implying that
568 the amino acid is especially present as a zwitterion (Aisawa *et al*., 2004), though the very
569 reactive metal oxide minerals in this approach are less relevant to early Earth scenarios.

570 At pH 9 and 11, for the Mg_2Al-LDH, the Langmuir isotherm plateaus at the maximum
571 anion exchange capacity of 0.5 mol Asp / mol Al, shown in **Figure 3**, indicating that all the
572 chloride has been exchanged (as Al/Cl = 1) and that the intercalated aspartates is all present
573 with a charge of -2. The Mg_3Al-LDH isotherm, **Figure 3b**, also shows a maximum anion
574 exchange capacity of 0.5 mol Asp/mol Al, though attained at higher initial solution
575 concentrations of Asp. These results establish that the Asp is taken up by LDH-Cl minerals
576 via an anion exchange process and not via surface/edge site adsorption, otherwise we would
577 expect to see adsorption amounts above the anion exchange capacity, and the adsorption to be
578 invariant of Mg/Al ratio. Furthermore, the concentration of amino acids by LDH-type
579 minerals requires alkaline conditions to be present, as the protonated zwitterion amino
580 carrying aspartate was not taken up at pH 7. This is explored further below.

581 At higher pH, the relative proportion of aspartate -1 (i.e. with a protonated amino
582 group) to aspartate -1 anions can be calculated to be: pH 9 = 20.1% of Asp -2 and 79.9% of
583 Asp -1; pH 11 = 96.2% of Asp -2 and 3.8% of Asp -1. It might therefore be expected that at

584 pH 9 significantly less amino acid would be removed from solution by the LDH mineral. In
585 fact, the adsorption isotherms for both materials suggest that all the intercalated aspartate is
586 present as Asp -2, even when the bulk solution pH was 9 (**Figure 3**). **Figure A1 (SI)** shows
587 the calculated quantity of Asp -2 and Asp -1 available in solution at pH 9 versus the measured
588 quantity of aspartate anions present in the LDH at maximum exchange. From the position of
589 the two series of points representing the adsorption isotherms, it can be noted that for the
590 same number of available interlayer sites and for a given initial concentration, twice as many
591 anions are intercalated in the Mg_2Al, when compared to Mg_3Al LDHs.

592 It is likely that once Asp -2 is preferentially exchanged, depleting the solution Asp -2
593 concentration, the solution aspartate re-equilibrates to generate more Asp -2 thus maintaining
594 the equilibrium ratio. The exchange reaction thus favours an increasing overall population of
595 Asp -2 at lower pH than would normally be expected. This mechanism does not operate at pH
596 7, where no exchange is observed, owing to the negligible amount of Asp -2 present, though
597 the effect appears to be cooperative and we speculate that once a non-negligible amount of
598 Asp -2 is present a tipping point is reached, whereupon the uptake of some Asp -2 results in a
599 positive feedback loop until all chloride exchange for Asp -2 is completed. Having established
600 that the uptake of the Asp -2 results in complete exchange for chloride such that dilute
601 solutions of aspartate may be concentrated to ~ 8 mol/L in the Mg_2Al-LDH, it would be
602 prescient to understand the interlayer arrangement of the biomolecule-mineral hybrid formed.

603 *5.2. The Interlayer Structure of Mg_RAl-Asp*

604 The structure of the interlayer of 2-dimensional layered mineral systems, such as LDHs, is
605 greatly affected by water content which varies according to the ambient relative humidity, it is
606 therefore important to assess the effect of water content during the characterisation process.

607 *Structure of Mg_2Al-Asp LDHs*. The XRD pattern and the FTIR spectra of the Mg_2Al-Asp
608 sample are presented in **Figure 5**. The cell parameters determined are reported in **Table 1**
609 along with the values calculated from the simulations. The basal *d*-spacing is influenced by
610 the interlayer water content. When the sample is fully dehydrated, the basal *d*-spacing was
611 found to be 8.76 Å, which is slightly greater than the theoretically determined value of 7.73
612 Å. The orientation of the amino acid with respect to the LDH sheets can be estimated using
613 simple geometry, as well as with computational chemistry methods, *vide infra*, based on the
614 aspartate long-axis dimension being 6.8 Å (calculated with Chemwindow 6.0). In Scheme 1
615 an angle of 0° relative to the LDH layer sheet corresponds to a vertical orientation of the
616 amino acid, and 90° to a vertical orientation. Extrapolating, the experimental data infers an
617 angle of 36° relative to the sheet, compared with the *c* value of 26°.

618 When water entered the interlayer domain, higher order basal reflections were
619 observed, suggesting a certain degree of order along the *c* direction. The *d*-spacing increases
620 to 12.01 Å when the interlayer domain was fully hydrated, implying a vertical orientation of
621 the intercalated amino acid. Although the trend of increasing *d*-spacing (and hence
622 crystallographic *c* parameter) with increasing hydration was identifiable in the simulations,
623 the increase was not as large as that observed experimentally.

624 This discrepancy between simulation and experiment is not unexpected, and is due to
625 an artefact of the periodic DFT modelling method, namely artificial electrostatic interactions
626 between the layers that are insufficiently screened by the interlayer species. Across the
627 surface of each layer of the model double hydroxide, the electron density varies according to

628 the atomic structure, and when these layers are placed opposite to one another and separated
629 by a vacuum there arise both Coulomb repulsions and dipolar attractions between the
630 separated layers. Lennard-Jones described the electrostatics of surfaces in 1928 (Lennard-
631 Jones and Dent, 1928), and they have since become well-known artefacts that occur when
632 modelling periodic systems (Geatches, 2011). Molecules placed into the interlayer effectively
633 screen the Coulomb repulsions, as indeed they do in the physical samples, but the dipole
634 attraction in the models remains somewhat undiminished, and creates an electrostatic field
635 between the layers, which affects the alignment of the interlayer molecules. In order to
636 completely negate this effect, which is solely due to the modelled electron density, further
637 screening between the layers (e.g. by the presence of more water molecules) would be
638 required.

639 Important changes in the intensities of the XRD lines can also be noted when the
640 hydration increases. From a crystallographic point of view in the hexagonal system, the (003)
641 reflection corresponds to the plane of cations and the (006) plane corresponds to the plane
642 located in the middle of the interlayer domain. Since the intensity of the XRD lines is
643 proportional to the electron density along these planes, a more complete description of the
644 interlayer organisation is gained by examining the evolution of the ratio I(003)/I(006). Both
645 the amino acid orientation and the location of the water molecules contribute to the electronic
646 density along the different planes. A precise description of the structure of the interlayer water
647 is thus possible only if the orientation of the amino acid is conserved. In the case where
648 changes in orientations of the amino acid are observed on addition of water molecules, no
649 detailed description can be carried out. This is the case when comparing the dehydrated
650 sample with the samples containing 2 water molecules per aspartate. As deduced above from
651 the analysis of the basal spacing, the orientation of the amino acid changes from a horizontal
652 orientation to a vertical orientation. The increase of the I(003)/I(0006) ratio can be therefore

attributed to the decrease in electron density in the (006) plane as a result of the lower electron density of the vertical amino acids. Such a scenario prevents a precise description of the position of the water molecules. However, when the hydration reaches 10 water molecules per aspartate, the orientation of the amino acid remains vertical, so that the only change in electron density along the planes comes from the water molecules. A strong increase of the I(003)/I(006) ratio strongly suggests that the water molecules orientate from the middle of the interlayer, strongly interacting with both the carboxylate groups or amino group of the amino acids and the hydroxyl groups of the layers. The same behaviour was also observed in the DFT simulations.

The FTIR spectra give further insight into the intra- and intermolecular interactions of the amino acid. Changes in the stretching frequency of the anti-symmetric and symmetric modes of the carboxylate groups ($\Delta\nu = \nu_{as} - \nu_{s}$) can be indicators of the binding configuration (Greiner *et al*., 2014; Roddick-Lanzilotta and McQuillan, 2000). The more asymmetric the interaction of the carbon-oxygen of the carboxylate group, the higher the difference in wave number between the anti-symmetric and symmetric stretching modes of the carboxylate. The general series $\Delta\nu_{unidentate} > \Delta\nu_{ionic} = \Delta\nu_{bridging} > \Delta\nu_{bidentate}$ was proposed and is supported by experimental work on metal chelate complexes. Given the LDH structure, it is unlikely that the amino acid would interact directly with the cations, but rather with the hydroxyl groups of the layer or with water molecules, if present, through hydrogen bonding, as observed in atomistic simulations by Kailinchev *et al*., 2010. Moreover, the interlayer domain is dynamic and this results in different interlayer arrangements for a given basal spacing and water content, as evidenced by our computer simulations, *vide infra*. For all these reasons, the series above cannot be directly applied to our system with sufficient confidence.

As noted above, the aspartate solution for pH 11 gives a $\Delta\nu$ value of 164 cm^{-1}. Regardless of the water content, the $\Delta\nu$ for all three samples is in the range 155-183 cm^{-1},

678 very close to that of the aqueous species. This suggests that aspartate interacts only weakly
679 and mainly through hydrogen bonding. Such an interpretation is further supported by the
680 almost constant intensity of the vibrational bands. The most notable difference is observed
681 when varying the interlayer water content.

682 For the dehydrated sample, the interlayer *c*-dimension deduced from XRD analysis,
683 implies that the amino acid is orientated horizontally within the interlayer domain. Such a
684 configuration may favour either a bidentate (the two carboxylate oxygen interacting with one
685 hydroxyl group from the layer) or a bridging configuration (one oxygen atom interacting with
686 one hydroxyl from the upper layer, the other oxygen of the same carboxylate group
687 interacting with a hydroxyl group from the lower layer). Since the vibrational peaks are much
688 broader compared to those of aqueous aspartate, it is likely that both configurations are
689 present in the interlayer domain, and indeed this is also reflected by the simulated model
690 shown in **Figure 7a**. The observed $\Delta\nu$ was determined to be 183 cm^{-1}, slightly higher than
691 that of the aqueous aspartate and may indicate a stronger bonding with the hydroxyl layer.
692 When the sample was allowed to equilibrate with ambient relative humidity, the $\Delta\nu$ value
693 shifted down to 165 cm^{-1} while the vibrational band become slightly narrower, although still
694 broader that those of aqueous aspartate. This phenomenon may be related to the abrupt
695 expansion of the interlayer spacing and subsequent re-organization of the interlayer amino
696 acid**.** A bridging configuration of the amino acid is no longer possible, but a unidentate (one
697 oxygen atom of the carboxylate group interacting with the hydroxyl layer, the other
698 interacting with the interlayer species) or bidentate configuration remains plausible as
699 illustrated by the DFT models presented in **Figure 7c**. However, since the structure of the
700 interlayer domain is mainly governed by hydrogen bonding, these two configurations are
701 expected to produce very similar $\Delta\nu$ and may explain the lower band broadness observed in
702 the FTIR spectra. Further addition of water in the interlayer domain has no effect on the

703 stretching frequencies of the carboxylate group, thus indicating a similar bonding
704 environment (as expected) since the basal spacings remain constant. The vibrational bands
705 become narrower and are very comparable to those of aqueous aspartate. DFT models for the
706 related structure also show that for such interlayer water content, the amino group can form
707 hydrogen bonds to a LDH layer (**Figure 7c**), Further addition of water thus produces an
708 isotropic bonding environment, with all carboxylate groups being involved in hydrogen
709 bonding either with the hydroxyl layer or the water molecules.
710
711 *Structure of Mg3Al-Asp LDH*. The Mg_3Al-Asp samples are different from the Mg_2Al-Asp
712 samples. The XRD patterns and FTIR spectra of these samples for different relative humidity
713 levels are displayed in **Figure 6**. Unlike the XRD pattern of the Mg_2Al-Asp samples, a good
714 fit was obtained only if each XRD peak was split and fitted with two Lorentzians, suggesting
715 the presence of materials with two different types of interlayer organizations. The dehydrated
716 sample gives interlayer spacings of 8.44 Å and 7.89 Å that correspond to estimated aspartate
717 orientations of 32° and 27° respectively with respect to the hydroxyl sheet (**Scheme 1** and
718 **Table 2**), assuming a rigid aspartate molecule and the simulation studies reported here add
719 further insight.
720 The simulated models for this system gave an interlayer spacing of 8.56 Å in good
721 agreement with the experimental interlayer spacing. Negligible changes are observed when
722 the Mg_3Al-Asp sample is equilibrated at 25% relative humidity, the interlayer spacing
723 becoming 8.56 Å and 7.91 Å, which is very close to that of the dehydrated samples. The
724 simulated interlayer spacings for these models give an average, depending on the starting
725 configuration, value of 8.44 Å (DFT) and 8.40 Å for the MD simulation (**Table A4**), both are
726 in good agreement with the experimental values. Note that the initial orientation of the amino
727 acid in the DFT simulated structures has only a minor effect on the final, optimized

728 configurations, and the amino acid tends to be oriented with its long axis parallel to the layer
729 (**Figure 7**). These results suggest that the layer charge density of the LDH affects the
730 orientation of the amino acids at low hydration level. The experimental intensity ratio
731 I(003)/I(006) decreased when 2 water molecules per aspartate were added, which is correlated
732 with the increase of the electronic density along the (006) plane where water molecules are
733 more likely to be positioned given the restricted layer spacing, *vide supra*. A fully hydrated
734 interlayer space gives experimental values of 11.06 Å and 11.80 Å, supporting a vertical
735 orientation of the amino acid as was seen in the Mg_2Al-Asp sample. For the highest basal
736 spacing (11.80 Å) the I(003/I(006) ratio (4.58) corresponds very closely with that
737 experimentally determined for the highest basal spacing (12.01 Å) of the Mg_2Al-Asp (4.57)
738 which means that a very similar interlayer organisation has taken place even if the quantity of
739 interlayer water is slightly different (10 and 7 water molecules in the Mg_2Al-Asp and Mg_3Al-
740 Asp structures respectively). While the orientation of the amino acid is governed mainly by
741 the layer charge density, the interlayer water structure is ruled by the orientation of the amino
742 acid.

743 The presence of the two interlayer structures at a given hydration state is also shown
744 by analysis of the FTIR spectra. While the position of the stretching modes of the carboxylate
745 groups is very comparable to those determined in the Mg_2Al-Asp sample, their width is
746 obviously greater. The two interlayer structures are thus averaged in the FTIR spectra
747 observed for the samples and this makes interpretation more complicated. Unfortunately, no
748 obvious changes can be observed when varying the hydration, with the band position and
749 width remaining similar. Based on the interpretation of the FTIR spectra on the Mg_2Al-Asp
750 sample, and given the restricted interlayer spacing, low interlayer hydration would favour a
751 bidentate or bridging configuration via hydrogen bonding (**Figure 7d**). In addition to the
752 inherent difficulty provided by the two interlayer structures, a band located at 1360 cm^{-1}

753 assigned to the anti-symmetric stretching modes of carbonate is present. The carbonate LDH
754 gives an interlayer spacing of around 7.8 Å and therefore should overlap with the XRD
755 pattern of the phases with low levels of hydration. As demonstrated by Iyi *et al*. carbonate
756 LDH does not exhibit any swelling properties, the interlayer spacing remaining unchanged
757 whatever the relative humidity (Iyi *et al*., 2007). Since no XRD lines corresponding to a basal
758 spacing of 7.8 Å are observed in the fully hydrated phase, the presence of carbonate phases
759 can be ruled out in our samples. Interestingly, the FTIR spectra of the fully hydrated sample
760 present new vibrational bands located at 1320 and 1450 cm^{-1} that were also found in the FTIR
761 spectra of aqueous aspartate at pH 7 or 9. These two bands can therefore be assigned to the
762 amino group in a protonated form. However, the stretching frequencies of the carboxylate
763 groups do not present the characteristic shift in wavenumbers associated with the presence of
764 the protonated amino group. This suggests that the aspartate is still charged -2 but with its
765 amino group strongly involved in the hydrogen bonding network. Looking at the structures in
766 **Figure 7e** and **7f**, it can be seen the amino group interacts more strongly with the hydroxyl
767 layer when it is slightly tilted in the interlayer domain (**Figure 7e**) as compared with pure
768 vertical orientation (**Figure 7f**).

769 *5.3. Dynamics of the interlayer*

770 Layered double hydroxides exist naturally, with a Mg_3Al-X structure being found in the
771 commonest form of hydrotalcite. This Mg:Al ratio thus seems to be favoured in nature and
772 should offer a greater stability than the Mg_2Al-X structure. This peculiarity may have been
773 conserved throughout time, so that even on the early Earth, most of the compounds from the
774 layered double hydroxides family may have been formed with the Mg_3Al-X structure. The
775 interlayer structure of the Mg_3Al-Asp sample was thus further investigated by molecular
776 dynamics at ambient conditions on large systems, allowing the sampling of numerous
777 structures and their interactions with the inclusion of thermal motions. Such a study addresses

778 the question of whether or not the interlayer domain of LDHs can act as a template for the
779 formation of peptides (Greenwell and Coveney, 2006).

780 MD analysis strongly supports our experimental data and enables further examination
781 of the potential reactivity of the LDH phase toward the formation of peptides. In **Figure 11**
782 we show the rapid increase in the potential reactive pairs, as the hydration drops below 5
783 waters per aspartate (totalling to 30% of all pairs). However, the interlayer domain does not
784 present any regio-specificity since both α-peptide and β-peptide linkages are counted in
785 similar quantities (~15%). It is likely that such selectivity is a matter of a reaction pathway
786 and should be further studied with *ab initio* mechanistic methods. Our results demonstrate that
787 peptide bond formation can occur in the interlayer domain of LDHs, and that is it more likely
788 to occur in a dehydrated state than in aqueous solution, showing the potential importance of
789 wetting/drying cycles.

790

791 # 6. Conclusions

792 We have examined the sorption of aspartate into layered double hydroxides. Our studies have
793 shown that, contrary to previous studies (Aisawa *et al*., 2004), it is possible to anion-exchange
794 chloride-LDHs with amino acids at up to 100% of the anion exchange capacity by using
795 alkaline pH conditions, giving an interlayer amino acid concentration of 7.93 mol/L starting
796 from a very dilute solution (0.020 mol/L). Under geochemical conditions, it may be
797 postulated that other anions may compete with the amino acids, though even at pH where
798 considerable OH- species are present, full exchange occurs. The strong affinity of LDH
799 toward carbonate anions may restrict its anionic exchange capacity and the overall interlayer
800 structure of the hybrid Mg_RAl-Asp system may be altered concomitantly. Therefore, in order
801 to attain maximum adsorption and concentration of amino acids in layered minerals, the most
802 plausible geochemical environments on the early Earth will be those with low dissolved CO_2

803 (and hence low carbonate), alkaline pH to ensure the amino acids are fully anionic and a pH
804 gradient where layered hydroxide minerals precipitate. Such environments may have been
805 low-medium temperature alkaline hydrothermal seeps, systems also suggested as providing
806 chemical and energetic gradients by Russell and co-workers (Martin *et al*., 2008; Martin and
807 Russell, 2007; Russell *et al*., 2013). The postulated abundance of LDHs on the early Earth
808 suggests a route by which peptides may have formed abiotically.

809 In the present study, the potential for layered double hydroxide minerals to act as hosts
810 for the concentration of the amino acid aspartate from solution has been studied, and the
811 structure of the host-guest systems elucidated. Starting from Mg_RAl-Cl LDH, it was found
812 that the chloride anions can be completely exchanged by aspartate anions at alkaline pH. The
813 interlayer structures of the LDH-Asp containing various interlayer water contents were
814 investigated by means of FTIR and XRD analysis coupled with electronic structure and
815 atomistic computer simulations. As suggested by the adsorption isotherm, the interlayer
816 aspartate molecules are present as dianions. The orientation of the amino acid within the
817 interlayer is found to be mainly influenced by the layer charge density and to a lesser extent,
818 by the interlayer water content, especially at high hydration levels. In general, low interlayer
819 hydration produces a horizontal orientation of the amino acid, with the long axis being
820 parallel to the layer, while high hydration levels induce a near-vertical orientation of the
821 amino acid. For intermediate interlayer water contents, i.e. 2 water molecules per aspartate, it
822 was observed that the layer charge density has a decisive role on the interlayer organisation,
823 with a higher layer charge density inducing a more vertical orientation of the amino acid.

824 Molecular dynamic simulations of LDH show that peptide formation can occur in the
825 interlayer domain of layered double hydroxides if the interlayer hydration is low, i.e. lower
826 than 5 water molecules per aspartate anion. Future studies will explore whether amide bond
827 formation can be attained without the need for heating, for example, through dehydrating

828 reagents such as carbonyl sulphide (COS) (Leman *et al*., 2004) to illustrate that both
829 concentrating and reaction mechanisms can occur at high pH in layered minerals, thus
830 providing insight into whether low temperature alkaline seeps may have been plausible
831 geochemical environments for abiotic peptide formation.
832

833 ## 6. Acknowledgements

834 The authors wish to acknowledge the Leverhulme Foundation (VE, DGF, HCG, BG) for the
835 funding that enabled this work. Computational resources were via HeCTOR (EPSRC
836 EP/K013718/1). We wish to thank Professor Cedric Carteret for many useful discussions
837 related to this work and HCG would like to thank Professor Gustaf Arrhenius for sharing his
838 extensive knowledge and insight into this area, and the Royal Society for further funding. BG
839 and DGF would like to thank Monica Price from the Oxford University Museum of Natural
840 History and Phil Wiseman from the Chemistry Research Laboratory of the University of
841 Oxford for giving access to FTIR and XRD facilities. VE would like to thank Matteo
842 Degiacomi from Chemistry Research Laboratory of the University of Oxford for discussion
843 and help in development of the analysis scripts.

References

Aimoz, L., Taviot-Guého, C., Churakov, S. V., Chukalina, M., Dähn, R., Curti, E., Bordet, P., and Vespa, M., (2012). Anion and Cation Order in Iodide-Bearing Mg/Zn–Al Layered Double Hydroxides. *J. Phys. Chem. C* **116**, 5460-5475.

Aisawa, S., Kudo, H., Hoshi, T., Takahashi, S., Hirahara, H., Umetsu, Y., and Narita, E., (2004). Intercalation behavior of amino acids into Zn–Al-layered double hydroxide by calcination–rehydration reaction. *J. Solid State Chem.* **177**, 3987-3994.

Arrhenius, G. O., (2003). Crystals and Life. *Helv. Chim. Acta* **86**, 1569-1586.

Baross, J. and Hoffman, S., (1985). Submarine hydrothermal vents and associated gradient environments as sites for the origin and evolution of life. *Origins Life Evol. Biosphere* **15**, 327-345.

Basiuk, V. A. and Sainz-Rojas, J., (2001). Catalysis of peptide formation by inorganic oxides: High efficiency of alumina under mild conditions on the earth-like planets. *Adv. Space Res.* **27**, 225-230.

Bellotto, M., Rebours, B., Clause, O., Lynch, J., Bazin, D., and Elkaïm, E., (1996). A reexamination of hydrotalcite crystal chemistry *J. Phys. Chem.* **100**, 8527-8534.

Berendsen, H. J. C., Postma, J. P. M., van Gunsteren, W. F., and Hermans, J., (1981). Interaction Models for Water in Relation to Protein Hydration. In: Pullman, B. (Ed.), *Intermolecular Forces*. Springer Netherlands.

Bernal, J. D., (1949). The Physical Basis of Life. *Proceedings of the Physical Society. Section B* **62**, 752.

Boulet, P., Greenwell, H. C., Stackhouse, S., and Coveney, P. V., (2006). Recent advances in understanding the structure and reactivity of clays using electronic structure calculations. *J. Mol. Struct.* **762**, 33-48.

Bujdák, J. and Rode, B. M., (1997). Silica, Alumina, and Clay-Catalyzed Alanine Peptide Bond Formation. *J. Mol. Evol.* **45**, 457-466.

Bujdak, J., Slosiarikova, H., Texler, N., Schwendinger, M., and Rode, B. M., (1994). On the possible role of montmorillonites in prebiotic peptide formation. *Monatshefte für Chemie / Chemical Monthly* **125**, 1033-1039.

Chen, Q., Shi, S., Liu, X., Jin, L., and Wei, M., (2009). Studies on the oxidation reaction of l-cysteine in a confined matrix of layered double hydroxides. *Chem. Eng. J.* **153**, 175-182.

Clark, S. J., Segall, M. D., Pickard, C. J., Hasnip, P. J., Probert, M. I. J., Refson, K., and Payne, M. C., (2005). First principles methods using CASTEP. *Zeitschrift fur Kristallographie* **220**, 567-570.

Coveney, P. V., Swadling, J. B., Wattis, J. A. D., and Greenwell, H. C., (2012). Theory, modelling and simulation in origins of life studies. *Chem. Soc. Rev.* **41**, 5430-5446.

Cygan, R. T., Liang, J.-J., and Kalinichev, A. G., (2004). Molecular Models of Hydroxide, Oxyhydroxide, and Clay Phases and the Development of a General Force Field. *The Journal of Physical Chemistry B* **108**, 1255-1266.

Cygan, R. T., Liang, J.-J., and Kalinichev, A. G., (2004). Molecular Models of Hydroxide, Oxyhydroxide, and Clay Phases and the Development of a General Force Field. *J. Phys. Chem. B* **108**, 1255-1266.

Davidson, E. R. and Chakravorty, S., (1992). A test of the Hirshfeld definition of atomic charges and moments. *Theor. Chim. Acta* **83**, 319-330.

Duan, X. and Evans, D. G., (2006). *Layered Double Hydroxides*. Springer.

Engel, M. H. and Nagy, B., (1982). Distribution and enantiomeric composition of amino acids in the Murchison meteorite. *Nature* **296**, 837-840.

Ferris, J. P. and Hagan Jr, W. J., (1984). HCN and chemical evolution: The possible role of cyano compounds in prebiotic synthesis. *Tetrahedron* **40**, 1093-1120.

Fitz, D., Reiner, H., and Rode, B. M., (2007). Chemical evolution toward the origin of life. *Pure Appl. Chem.* **79**, 2101-2117.

Fraser, D. G., Fitz, D., Jakschitz, T., and Rode, B. M., (2011). Selective adsorption and chiral amplification of amino acids in vermiculite clay-implications for the origin of biochirality. *PCCP* **13**, 831-838.

Fraser, D. G., Greenwell, H. C., Skipper, N. T., Smalley, M. V., Wilkinson, M. A., Deme, B., and Heenan, R. K., (2011). Chiral interactions of histidine in a hydrated vermiculite clay. *PCCP* **13**, 825-830.

Fudala, Á., Pálinkó, I., and Kiricsi, I., (1999). Preparation and Characterization of Hybrid Organic−Inorganic Composite Materials Using the Amphoteric Property of Amino Acids: Amino Acid Intercalated Layered Double Hydroxide and Montmorillonite. *Inorg. Chem.* **38**, 4653-4658.

Geatches, D., (2011). Clay minerals and their gallery guests. PhD thesis. Durham University.

Gilbert, W., (1986). Origin of life: The RNA world. *Nature* **319**, 618-618.

Greenwell, H. and Coveney, P. V., (2006). Layered Double Hydroxide Minerals as Possible Prebiotic Information Storage and Transfer Compounds. *Origins Life Evol. Biosphere* **36**, 13-37.

Greenwell, H. C., Jones, W., Coveney, P. V., and Stackhouse, S., (2006). On the application of computer simulation techniques to anionic and cationic clays: A materials chemistry perspective. *J. Mater. Chem.* **16**, 708.

Grégoire, B., Ruby, C., and Carteret, C., (2012). Structural Cohesion of MII-MIII Layered Double Hydroxides Crystals: Electrostatic Forces and Cationic Polarizing Power. *Cryst. Growth Des.* **12**, 4324-4333.

Greiner, E., Kumar, K., Sumit, M., Giuffre, A., Zhao, W., Pedersen, J., and Sahai, N., (2014). Adsorption of l-glutamic acid and l-aspartic acid to γ-Al2O3. *Geochim. Cosmochim. Acta* **133**, 142-155.

Grimme, S., (2006). Semiempirical GGA-type density functional constructed with a long-range dispersion correction. *J. Comput. Chem.* **27**, 1787-1799.

Hall, D. O., Cammack, R., and Rao, K. K., (1971). Role for Ferredoxins in the Origin of Life and Biological Evolution. *Nature* **233**, 136-138.

Hanczyc, M. M., Fujikawa, S. M., and Szostak, J. W., (2003). Experimental Models of Primitive Cellular Compartments: Encapsulation, Growth, and Division. *Science* **302**, 618-622.

Hashizume, H., Theng, B. K. G., and Yamagishi, A., (2002). Adsorption and discrimination of alanine and alanyl-alanine enantiomers by allophane. *Clay Miner.* **37**, 551-557.

Hazen, R. M. and Sverjensky, D. A., (2010). Mineral Surfaces, Geochemical Complexities, and the Origins of Life. *Cold Spring Harbor Perspectives in Biology* **2**.

Head, J. D. and Zerner, M. C., (1985). A Broyden-Fletcher-Goldfarb-Shanno optimization procedure for molecular geometries. *Chem. Phys. Lett.* **122**, 264-270.

Hernandez, A. R. and Piccirilli, J. A., (2013). Chemical origins of life: Prebiotic RNA unstuck. *Nat Chem* **5**, 360-362.

Hess, B., Kutzner, C., van der Spoel, D., and Lindahl, E., (2008). GROMACS 4: Algorithms for Highly Efficient, Load-Balanced, and Scalable Molecular Simulation. *J. Chem. Theory Comput.* **4**, 435-447.

Hibino, T., (2004). Delamination of Layered Double Hydroxides Containing Amino Acids. *Chem. Mater.* **16**, 5482-5488.

Hines, D. R., Solin, S. A., Costantino, U., and Nocchetti, M., (2000). Physical properties of fixed-charge layer double hydroxides. *Phys. Rev. B* **61**, 11348-11358.

Hofmeister, W. and Platen, H. V., (1992). Crystal Chemistry and Atomic Order in Brucite-related Double-layer Structures. *Crystallogr. Rev.* **3**, 3-26.

944 Iyi, N., Fujii, K., Okamoto, K., and Sasaki, T., (2007). Factors influencing the hydration of
945 layered double hydroxides (LDHs) and the appearance of an intermediate second
946 staging phase. *Appl*. *Clay Sci*. **35**, 218-227.
947 Iyi, N., Yamada, H., and Sasaki, T., (2011). Deintercalation of carbonate ions from carbonate-
948 type layered double hydroxides (LDHs) using acid–alcohol mixed solutions. *Appl*.
949 *Clay Sci*. **54**, 132-137.
950 Kalinichev, A. G., Kumar, P. P., and Kirkpatrick, R. J., (2010). Molecular dynamics computer
951 simulations of the effects of hydrogen bonding on the properties of layered double
952 hydroxides intercalated with organic acids. *Philos*. *Mag*. **90**, 2475-2488.
953 Kelley, D. S., Karson, J. A., Blackman, D. K., Fruh-Green, G. L., Butterfield, D. A., Lilley,
954 M. D., Olson, E. J., Schrenk, M. O., Roe, K. K., Lebon, G. T., Rivizzigno, P., and the,
955 A. T. S. P., (2001). An off-axis hydrothermal vent field near the Mid-Atlantic Ridge at
956 30[deg] N. *Nature* **412**, 145-149.
957 Kelley, D. S., Karson, J. A., Früh-Green, G. L., Yoerger, D. R., Shank, T. M., Butterfield, D.
958 A., Hayes, J. M., Schrenk, M. O., Olson, E. J., Proskurowski, G., Jakuba, M., Bradley,
959 A., Larson, B., Ludwig, K., Glickson, D., Buckman, K., Bradley, A. S., Brazelton, W.
960 J., Roe, K., Elend, M. J., Delacour, A., Bernasconi, S. M., Lilley, M. D., Baross, J. A.,
961 Summons, R. E., and Sylva, S. P., (2005). A Serpentinite-Hosted Ecosystem: The Lost
962 City Hydrothermal Field. *Science* **307**, 1428-1434.
963 Kuma, K., Paplawsky, W., Gedulin, B., and Arrhenius, G., (1989). Mixed-valence hydroxides
964 as bioorganic host minerals. *Origins Life Evol*. *Biosphere* **19**, 573-601.
965 Kumar, P. P., Kalinichev, A. G., and Kirkpatrick, R. J., (2006). Hydration, Swelling,
966 Interlayer Structure, and Hydrogen Bonding in Organolayered Double Hydroxides:
967 Insights from Molecular Dynamics Simulation of Citrate-Intercalated Hydrotalcite. *J*.
968 *Phys*. *Chem*. *B*. **110**, 3841-3844.
969 Kumar, P. P., Kalinichev, A. G., and Kirkpatrick, R. J., (2007). Molecular Dynamics
970 Simulation of the Energetics and Structure of Layered Double Hydroxides Intercalated
971 with Carboxylic Acids. *J*. *Phys*. *Chem*. *C* **111**, 13517-13523.
972 Lambert, J.-F., (2008). Adsorption and Polymerization of Amino Acids on Mineral Surfaces:
973 A Review. *Origins of Life and Evolution of Biospheres* **38**, 211-242.
974 Lang, S. Q., Butterfield, D. A., Schulte, M., Kelley, D. S., and Lilley, M. D., (2010). Elevated
975 concentrations of formate, acetate and dissolved organic carbon found at the Lost City
976 hydrothermal field. *Geochim*. *Cosmochim*. *Acta* **74**, 941-952.
977 Lascelles, D. F., (2007). Black smokers and density currents: A uniformitarian model for the
978 genesis of banded iron-formations. *Ore Geology Reviews* **32**, 381-411.
979 Lee, M. H., (1996). PhD thesis. PhD Thesis. Cambridge University.
980 Leman, L., Orgel, L., and Ghadiri, M. R., (2004). Carbonyl Sulfide-Mediated Prebiotic
981 Formation of Peptides. *Science* **306**, 283-286.
982 Lennard-Jones, J. E. and Dent, B. M., (1928). Cohesion at a crystal surface. *Trans*. *Faraday*
983 *Soc*. **24**, 92-108.
984 MacKerell, A. D., Banavali, N., and Foloppe, N., (2000). Development and current status of
985 the CHARMM force field for nucleic acids. *Biopolymers* **56**, 257-265.
986 Martin, R., (2004). *Electronic structure: basic theory and practical methods*. Cambridge
987 University Press.
988 Martin, W., Baross, J., Kelley, D., and Russell, M. J., (2008). Hydrothermal vents and the
989 origin of life. *Nat*. *Rev*. *Microbiol*. **6**, 805-814.
990 Martin, W. and Russell, M. J., (2007). On the origin of biochemistry at an alkaline
991 hydrothermal vent. *Philos*. *T*. *Roy*. *Soc*. *B* **362**, 1887-1925.
992 Martra, G., Deiana, C., Sakhno, Y., Barberis, I., Fabbiani, M., Pazzi, M., and Vincenti, M.,
993 (2014). The Formation and Self-Assembly of Long Prebiotic Oligomers Produced by

994 the Condensation of Unactivated Amino Acids on Oxide Surfaces. *Angew. Chem. Int.*
995 *Ed.* **53**, 4671-4674.
996 McNellis, E. R., Meyer, J., and Reuter, K., (2009). Azobenzene at coinage metal surfaces:
997 Role of dispersive van der Waals interactions. *Phys. Rev. B: Condens. Matter* **80**.
998 Mejias, J. A., Berry, A. J., Refson, K., and Fraser, D. G., (1999). The kinetics and mechanism
999 of MgO dissolution. *Chem. Phys. Lett.* **314**, 558-563.
1000 Monkhorst, H. J. and Pack, J. D., (1976). Special points for Brillouin-zone integrations. *Phys.*
1001 *Rev. B* **13**, 5188-5192.
1002 Mulliken, R. S., (1955). Electronic population analysis on LCAO-MO molecular wave
1003 functions. I. *J. Chem. Phys.* **23**, 1833-1840.
1004 Mulliken, R. S., (1955). Electronic population analysis on LCAO-MO molecular wave
1005 functions. II. Overlap populations, bond orders, and covalent bond energies. *J. Chem.*
1006 *Phys.* **23**, 1841-1846.
1007 Mulliken, R. S., (1955). Electronic population analysis on LCAO-MO molecular wave
1008 functions. III. effects of hybridization on overlap and gross AO populations. *J. Chem.*
1009 *Phys.* **23**, 2338-2342.
1010 Mulliken, R. S., (1955). Electronic population analysis on LCAO-MO molecular wave
1011 functions. IV. bonding and antibonding in LCAO and valence-bond theories. *J. Chem.*
1012 *Phys.* **23**, 2343-2346.
1013 Newman, S. P., Williams, S. J., Coveney, P. V., and Jones, W., (1998). Interlayer
1014 Arrangement of Hydrated MgAl Layered Double Hydroxides Containing Guest
1015 Terephthalate Anions: Comparison of Simulation and Measurement. *J. Phys. Chem. B*
1016 **102**, 6710-6719.
1017 Pálinkó, I., (2006). Organic-Inorganic Nanohybrids of Biologically Important Molecules and
1018 Layered Double Hydroxides. *Nanopages* **1**, 295-314.
1019 Patel, B. H., Percivalle, C., Ritson, D. J., DuffyColm, D., and Sutherland, J. D., (2015).
1020 Common origins of RNA, protein and lipid precursors in a cyanosulfidic
1021 protometabolism. *Nat Chem* **7**, 301-307.
1022 Perdew, J. P., Burke, K., and Ernzerhof, M., (1996). Generalized gradient approximation
1023 made simple. *Phys. Rev. Lett.* **77**, 3865-3868.
1024 Pisson, J., Morel-Desrosiers, N., Morel, J. P., de Roy, A., Leroux, F., Taviot-Guého, C., and
1025 Malfreyt, P., (2011). Tracking the Structural Dynamics of Hybrid Layered Double
1026 Hydroxides. *Chem. Mater.* **23**, 1482-1490.
1027 Plankensteiner, K., Righi, A., Rode, B. M., Gargallo, R., Jaumot, J., and Tauler, R., (2004).
1028 Indications towards a stereoselectivity of the salt-induced peptide formation reaction.
1029 *Inorg. Chim. Acta* **357**, 649-656.
1030 Powner, M. W., Gerland, B., and Sutherland, J. D., (2009). Synthesis of activated pyrimidine
1031 ribonucleotides in prebiotically plausible conditions. *Nature* **459**, 239-242.
1032 Reinholdt, M. X., Babu, P. K., and Kirkpatrick, R. J., (2009). Preferential Adsorption of
1033 Lower-Charge Glutamate Ions on Layered Double Hydroxides: An NMR
1034 Investigation. *J. Phys. Chem. C* **113**, 3378-3381.
1035 Richardson, I. G., (2013). The importance of proper crystal-chemical and geometrical
1036 reasoning demonstrated using layered single and double hydroxides. *Acta Crystallogr.*
1037 *Sect. B: Struct. Sci.* **69**, 150-162.
1038 Rimola, A., Sodupe, M., and Ugliengo, P., (2007). Aluminosilicate Surfaces as Promoters for
1039 Peptide Bond Formation: An Assessment of Bernal's Hypothesis by ab Initio
1040 Methods. *J. Am. Chem. Soc.* **129**, 8333-8344.
1041 Roddick-Lanzilotta, A. D. and McQuillan, A. J., (2000). An in situ Infrared Spectroscopic
1042 Study of Glutamic Acid and of Aspartic Acid Adsorbed on TiO2: Implications for the
1043 Biocompatibility of Titanium. *J. Colloid Interface Sci.* **227**, 48-54.

Rode , B. M., (1999). Peptides and the origin of life. *Peptides* **20**, 773-786.
Russell, M. J., (2003). The Importance of Being Alkaline. *Science* **302**, 580-581.
Russell, M. J., Nitschke, W., and Branscomb, E., (2013). The inevitable journey to being. *Philos. T. Roy. Soc. B* **368**.
Sanchez-Portal, D., Artacho, E., and Soler, J. M., (1995). Projection of plane-wave calculations into atomic orbitals. *Solid State Commun.* **95**, 685-690.
Schoonen, M., Smirnov, A., and Cohn, C., (2004). A Perspective on the Role of Minerals in Prebiotic Synthesis. *J. Hum. Environ. Syst* **33**, 539-551.
Schwendinger, M. G. and Rode, B. M., (1992). Investigations on the mechanism of the salt-induced peptide formation. *Origins Life Evol. Biosphere* **22**, 349-359.
Segall, M. D., Pickard, C. J., Shah, R., and Payne, M. C., (1996). Population analysis in plane wave electronic structure calculations. *Mol. Phys.* **89**, 571-577.
Segall, M. D., Shah, R., Pickard, C. J., and Payne, M. C., (1996). Population analysis of plane-wave electronic structure calculations of bulk materials. *Phys. Rev. B: Condens. Matter* **54**, 16317-16320.
Sleep, N. H., (2010). The Hadean-Archaean Environment. *Cold Spring Harbor Perspectives in Biology* **2**.
Thyveetil, M.-A., Coveney, P. V., Suter, J. L., and Greenwell, H. C., (2007). Emergence of Undulations and Determination of Materials Properties in Large-Scale Molecular Dynamics Simulation of Layered Double Hydroxides. *Chem. Mater.* **19**, 5510-5523.
Trave, A., Selloni, A., Goursot, A., Tichit, D., and Weber, J., (2002). First Principles Study of the Structure and Chemistry of Mg-Based Hydrotalcite-Like Anionic Clays. *J. Phys. Chem. B* **106**, 12291-12296.
Ugliengo, P., Zicovich-Wilson, C. M., Tosoni, S., and Civalleri, B., (2009). Role of dispersive interactions in layered materials: A periodic B3LYP and B3LYP-D* study of Mg(OH)2, Ca(OH)2 and kaolinite. *J. Mater. Chem.* **19**, 2564-2572.
Underwood, T., Erastova, V., Cubillas, P., and Greenwell, H. C., (2015). Molecular Dynamic Simulations of Montmorillonite–Organic Interactions under Varying Salinity: An Insight into Enhanced Oil Recovery. *J. Phys. Chem. C*.
Vanderbilt, D., (1990). Soft self-consistent pseudopotentials in a generalized eigenvalue formalism. *Phys. Rev. B* **41**, 7892-7895.
Wei, M., Yuan, Q., Evans, D. G., Wang, Z., and Duan, X., (2005). Layered solids as a "molecular container" for pharmaceutical agents: l-tyrosine-intercalated layered double hydroxides. *J. Mater. Chem.* **15**, 1197-1203.
Whilton, N. T., Vickers, P. J., and Mann, S., (1997). Bioinorganic clays: synthesis and characterization of amino- and polyamino acid intercalated layered double hydroxides. *J. Mater. Chem.* **7**, 1623-1629.
Wolpert, M. and Hellwig, P., (2006). Infrared spectra and molar absorption coefficients of the 20 alpha amino acids in aqueous solutions in the spectral range from 1800 to 500 cm−1. *Spectrochim. Acta A* **64**, 987-1001.

Tables

Insights into the Behaviour of Biomolecules on the Early Earth: The Concentration of Aspartate by Layered Double Hydroxide Minerals

Brian Grégoire[a], Valentina Erastova[b], Dawn L. Geatches[c], Stewart J. Clark[d], H. Christopher Greenwell[b*], Donald G. Fraser[a].

[a]Department of Earth Sciences, University of Oxford, South Parks Road, Oxford, OX1 3AN, UK
[b]Department of Earth Sciences, Durham University, South Road, Durham, DH1 3LE, UK
[c] Daresbury Laboratory (STFC), Warrington, WA4 4AD, UK
[d]Department of Physics, Durham University, South Road, Durham, DH1 3LE, UK

Table captions

Table 1: Experimental cell parameters, XRD intensity ratio and orientation angle of aspartate with respect to the hydroxyl surface along with the calculated values from DFT models with different interlayer water content in Mg_2Al-Asp.

Table 2 : Experimental cell parameters, XRD intensity ratio and orientation angle of aspartate with respect to the hydroxyl surface along with the calculated values from DFT and MD models with different interlayer water content in Mg_3Al-Asp.

Table 1

Mg_2Al-Asp H_2O/Asp	c_0 param (Å)	c param (Å)	I_{003}/I_{006}	Angle Θ_{exp} (°)	Calc. value (Å)	Angle Θ_{th} (°)
0 (Mg_2AlOH_6 $Asp_{1/2}$)	26.29	8.76	1,52	54	7.73	65
2 (Mg_2AlOH_6 $Asp_{1/2}$. 1H2O)	35.89	11.96	2.00	0	8.27	59
5 (Mg_2AlOH_6 $Asp_{1/2}$. 2.5H2O)	NA	NA	NA	NA	9.6[(1)]	45
7 (Mg_2AlOH_6 $Asp_{1/2}$. 3.5H2O)	36.03	12.01	4.57	0	NA	NA

Table 2

Mg_3Al-Asp H_2O/Asp	c_0 param (Å)	c param (Å)	I_{003}/I_{006}	Angle Θ_{exp} (°)	Calc. value (Å)	Angle Θ_{th} (°)
0 (Mg_3AlOH_8 $Asp_{1/2}$)	23.67 25.32	7.89 8.44	1,78 1.77	63 58	$7.73^{[DFT]}$ $8.4^{[MD]}$	65
2 (Mg_3AlOH_8 $Asp_{1/2}$. 1H2O)	23.72 25.69	7.91 8.56	1.24 0.85	63 56	$8.00^{[DFT](1)}$ $8.75^{[DFT](1)}$ $8.40^{[MD]}$	62 55
5 (Mg_3AlOH_8 $Asp_{1/2}$. 2.5H2O)	N.A	N.A	N.A	N.A	$9.53^{[DFT]\ [1)}$ $10.98^{[DFT]\ (1)}$	46 25
10 (Mg_2AlOH_6 $Asp_{1/2}$. 5H2O)	33.17 35.39	11.06 11.80	3.24 4.58	23 0	$10.65^{[MD]\ (3)}$	

(1) The two calculated basal spacing corresponds to the extreme values of the simulation cells starting with aspartate in different orientation

(2) Extracted from MD simulation on $Mg_3AlOH_8Asp_{1/2}.5H_2O$

Scheme

Insights into the Behaviour of Biomolecules on the Early Earth: The Concentration of Aspartate by Layered Double Hydroxide Minerals

Brian Grégoire[a], Valentina Erastova[b], Dawn L. Geatches[c], Stewart J. Clark[d], H. Christopher Greenwell[b*], Donald G. Fraser[a].

[a]Department of Earth Sciences, University of Oxford, South Parks Road, Oxford, OX1 3AN, UK
[b]Department of Earth Sciences, Durham University, South Road, Durham, DH1 3LE, UK
[c] Daresbury Laboratory (STFC), Warrington, WA4 4AD, UK
[d]Department of Physics, Durham University, South Road, Durham, DH1 3LE, UK

Scheme caption

Scheme 1: Estimation of the tilt angle (Θ) of the interlayer aspartate amino acid based on the experimental c parameters.

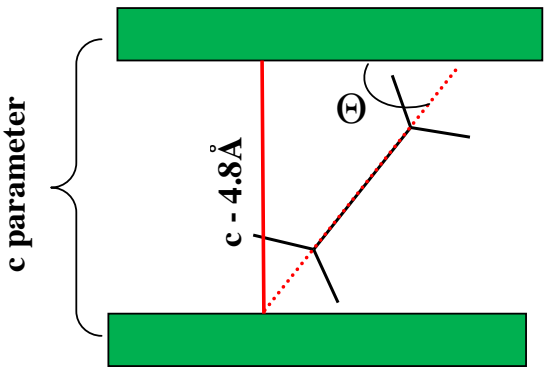

Scheme 1

Figures

Insights into the Behaviour of Biomolecules on the Early Earth: The Concentration of Aspartate by Layered Double Hydroxide Minerals

Brian Grégoire[a], Valentina Erastova[b], Dawn L. Geatches[c], Stewart J. Clark[d], H. Christopher Greenwell[b*], Donald G. Fraser[a].

[a]Department of Earth Sciences, University of Oxford, South Parks Road, Oxford, OX1 3AN, UK
[b]Department of Earth Sciences, Durham University, South Road, Durham, DH1 3LE, UK
[c] Daresbury Laboratory (STFC), Warrington, WA4 4AD, UK
[d]Department of Physics, Durham University, South Road, Durham, DH1 3LE, UK

Figures captions

Figure 1. A schematic to show the general structure of a layered double hydroxide mineral, illustrating how one set of interlayer anions may be exchanged for another, with the two-dimensional layered structure adapting to the increased size of the new guest molecule. The colour scheme is M^{3+} = dark grey; M^{2+} = green; O = red; N = blue; C = middle grey; H = white; Cl = pink.

Figure 2. Powder X-ray diffraction patterns for (a) Mg_2Al-X, and (b) Mg_3Al-X layered double hydroxide materials prepared, with the corresponding infra-red spectra, (c) for Mg_2Al-X, and (d) Mg_3Al-X. Where X = CO_3 or Cl.

Figure 3. Adsorption isotherms of aspartate for: (a) Mg_2Al-Cl, and (b) Mg_2Al-Cl. The plots show that at both Mg/Al ratios, the maximum adsorption capacity is around 1 aspartate per 2 Al, confirming aspartate is present as the doubly charged (2-) form.

Figure 4. ATR-FTIR spectra of (a) aspartate solution ([Asp] = 1M) at pH 7, 9 and 11 and (b) colloidal suspension of aspartate intercalated into the interlayer domain of 2:1 LDH at pH 9 and 11.

Figure 5. On the left the powder X-Ray diffraction patterns of Mg_2Al-Asp are shown at different interlayer water content. The right hand side shows the FTIR spectra of the same materials (Samples obtained from $[Asp]_0$ = 50 mM ; pH = 11 ; Contact time = 20 h)

Figure 6. On the left the powder X-Ray diffraction patterns of Mg_3Al-Asp are shown at different interlayer water content. The right hand side shows the FTIR spectra of the same materials (Samples obtained from $[Asp]_0$ = 50 mM ; pH = 11 ; Contact time = 20 h)

Figure 7. DFT optimised Mg_2Al-Asp (a-c) and Mg_3Al-Asp (d-f) structures containing (a,d) 0 water molecule par aspartate, (b,e) 2 water molecules per aspartate and (c,f) 5 water molecules per aspartate

Figure 8. Side view of a slice of the MD simulation box of LDH31 with charge balancing aspartate 2- and varying amounts of water: (a) 20 water molecules per aspartate, (b) 15 water molecules per aspartate, (c) 10 water molecules per aspartate, (d) 7 water molecules per aspartate, (e) 5 water molecules per aspartate, (f) 3 water molecules per aspartate, (g) 2 water molecules per aspartate and (h) no water. LDH31 is shown as VDW spheres, where pink is Mg, cyan is Al, red is O and white is H; Aspartate is shown as thick liquorice, where cyan is C, blue is N, red is O and white is H, water is shown as thin liquorice, where red is O and white is H. The top and bottom clay layer are given fully, while being a periodic copy.

Figure 9. The figures show alignment of the vector between (a) two oxygens of carboxyl group on side chain; (b) two oxygens on carboxyl group of the back bone; (c) between two carbons of the carboxyl group, the schematic vector assignment is given in (d). The angle is given with respect to the LDH layer. The colours are per system: 0 water system– red, 2 waters per aspartate – orange, 3 waters per aspartate – lime, 5 waters per aspartate – green, 7 waters per aspartate – light blue, 10 waters per aspartate – blue, 15 waters per aspartate – purple, 20 waters per aspartate – magenta.

Figure 10. possible reactive alignments of aspartate leading to (a) alpha-peptide, (b) beta-peptide and (c) cyclic structure that would prevent beta-peptide formation.

Figure 11. Expected quantity of peptides formed (%) within the interlayer gallery of LDH with various interlayer water content.

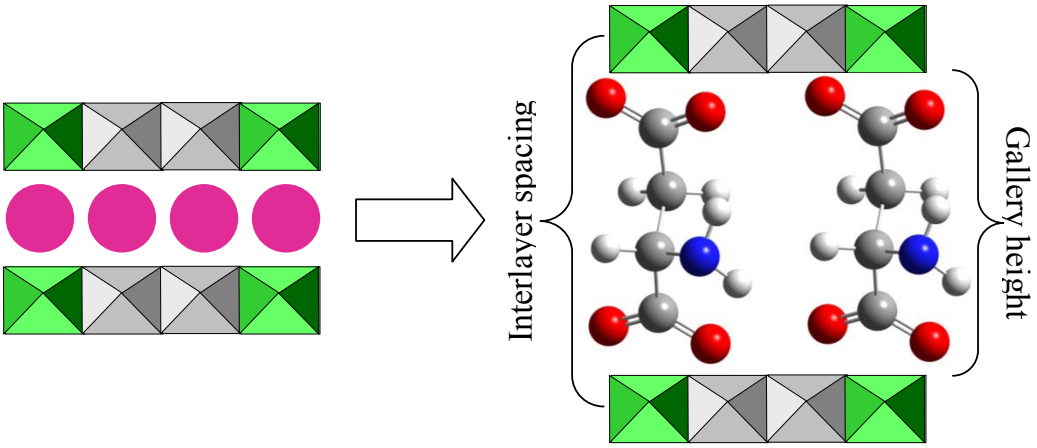

Figure 2

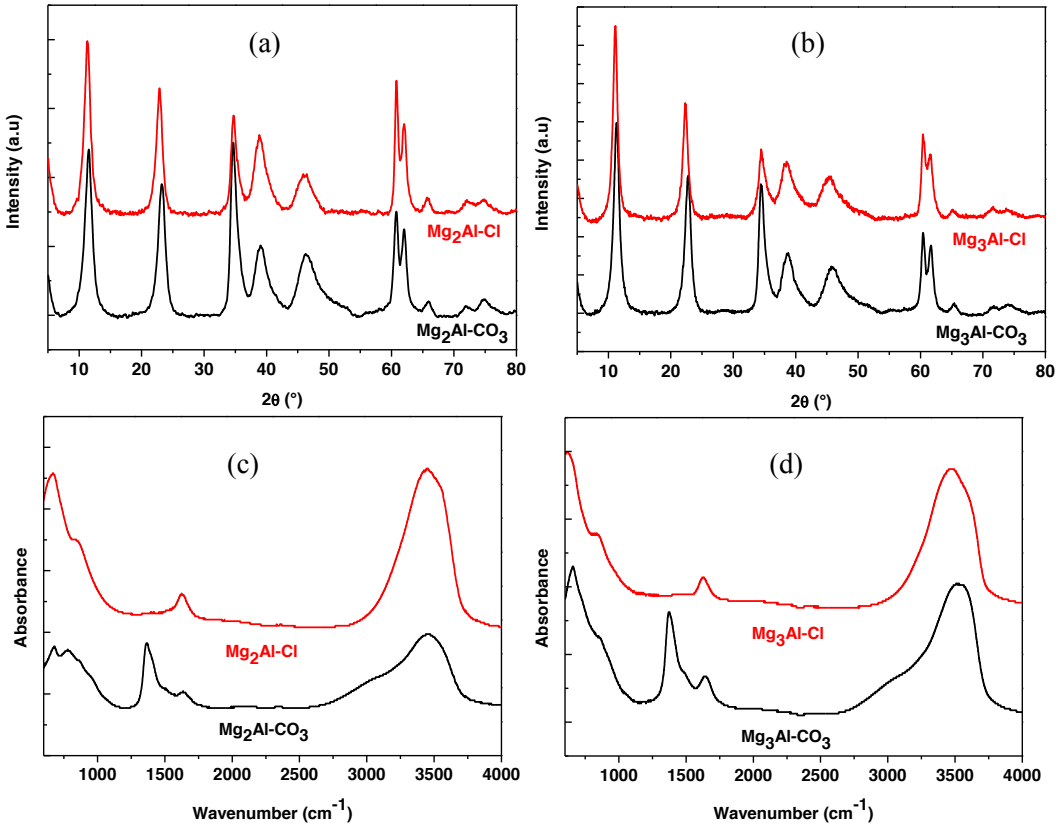

Figure 2

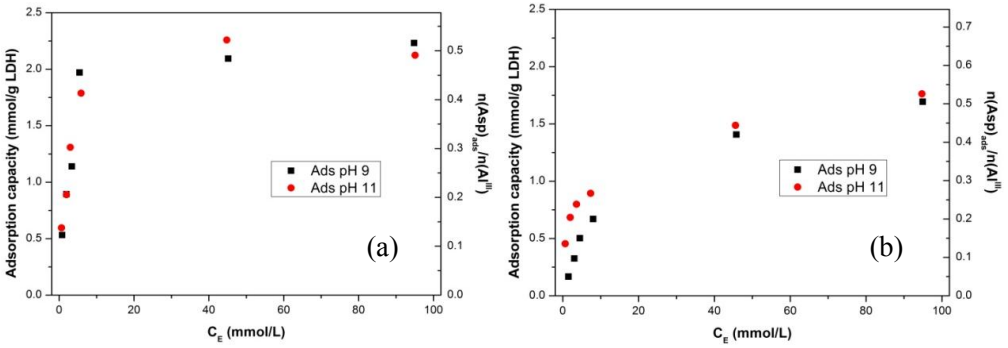

Figure 3

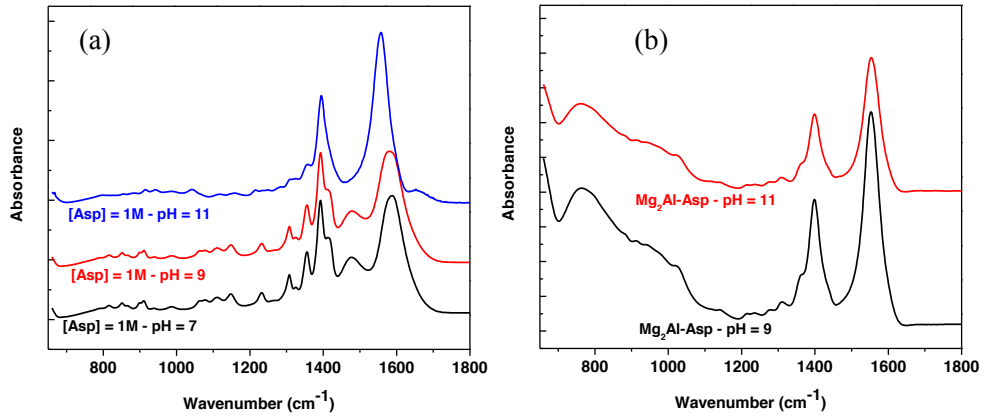

Figure 4

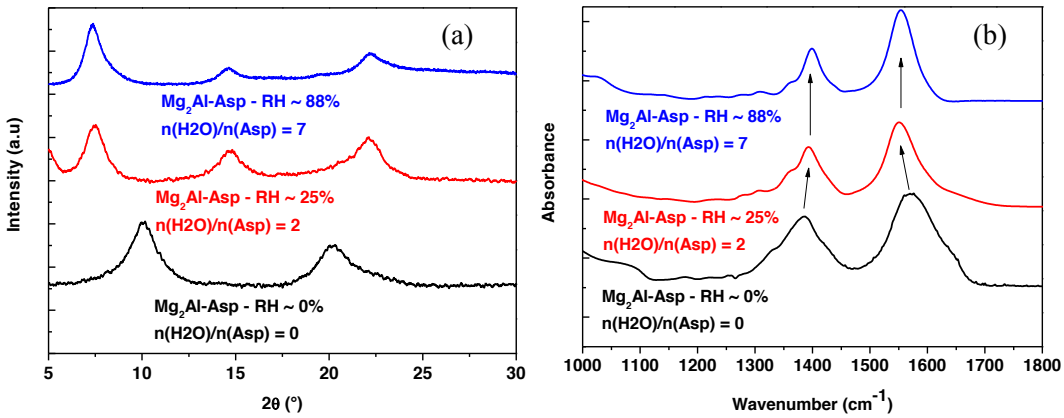

Figure 5

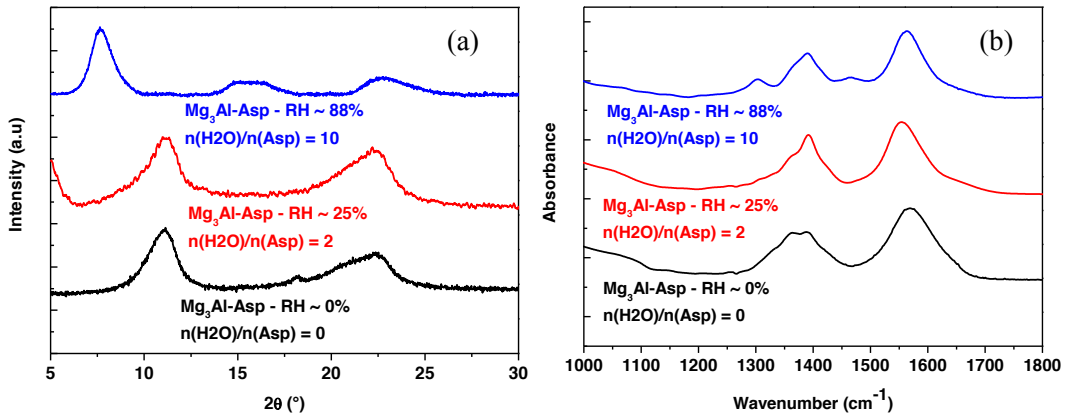

Figure 6

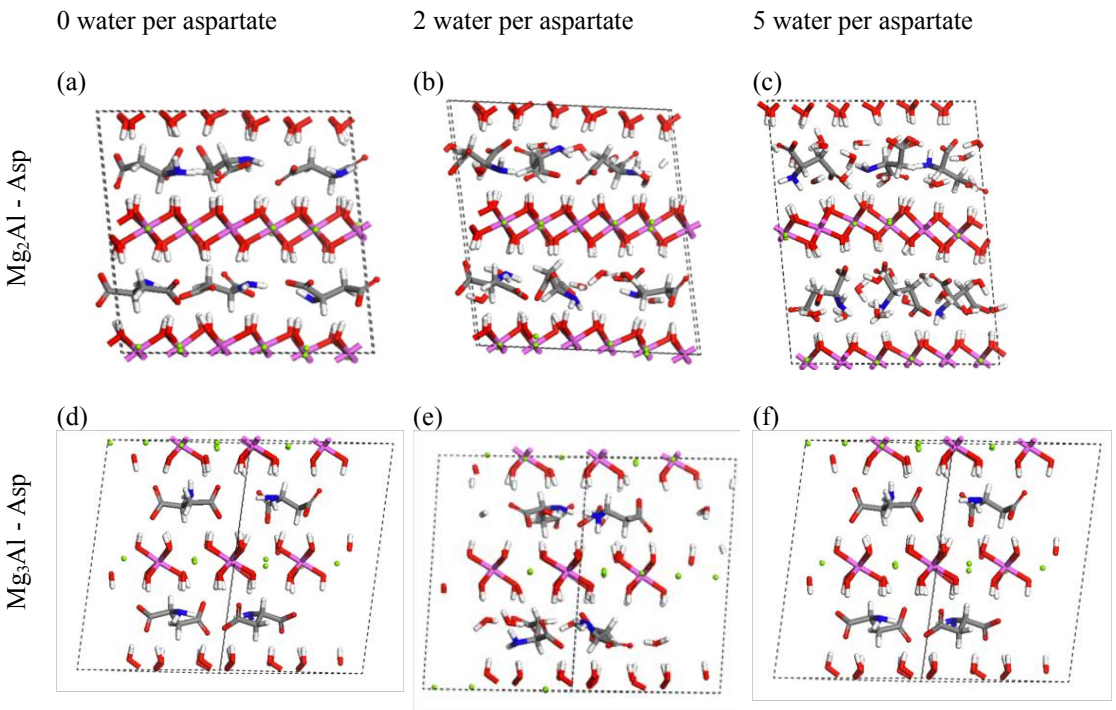

Figure 7

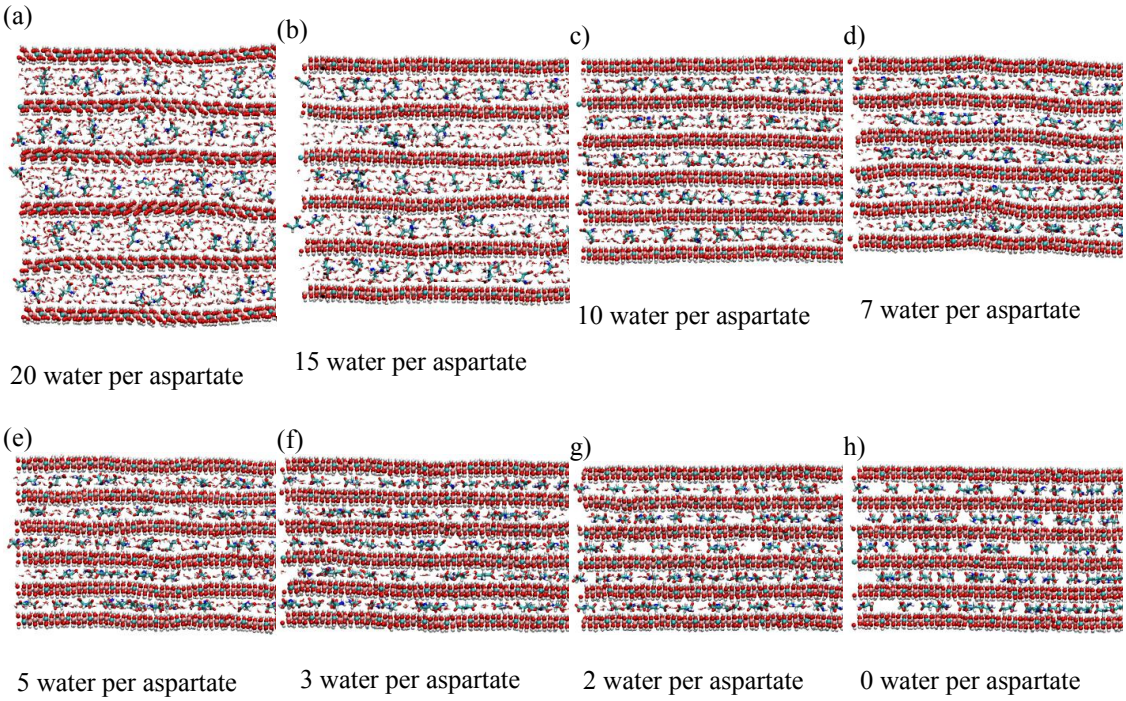

Figure 8

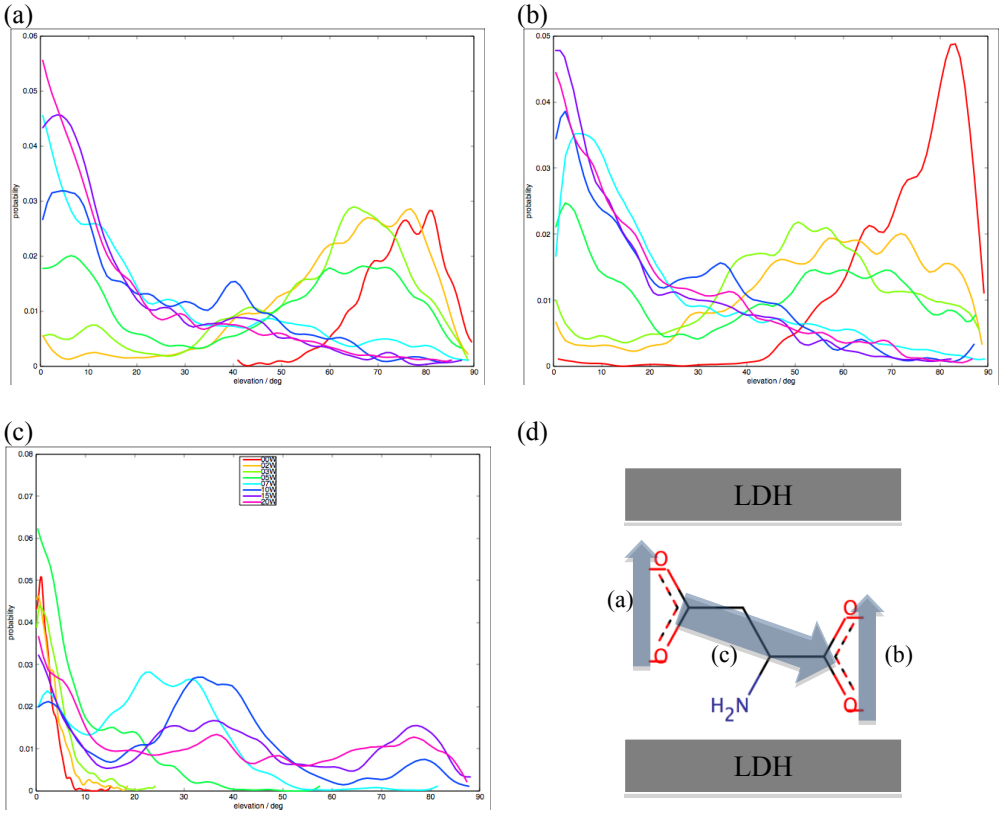

Figure 9

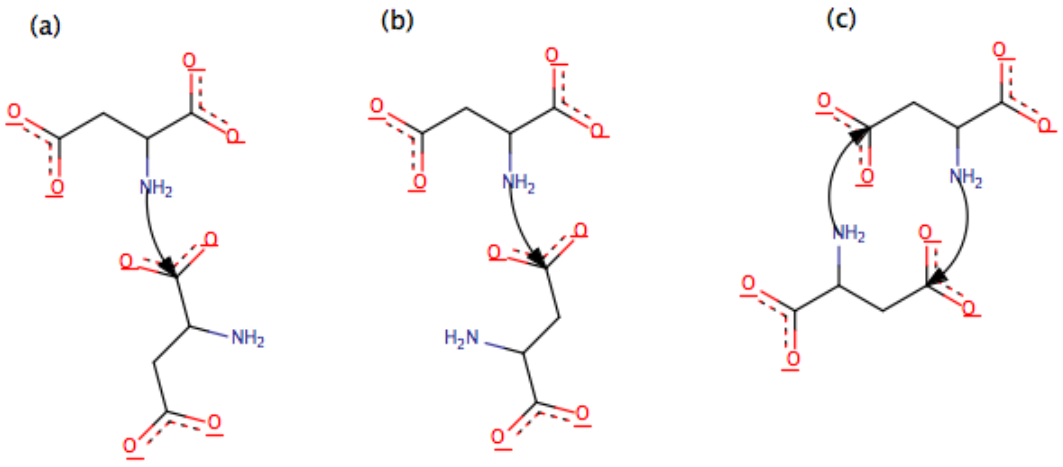

Figure 10

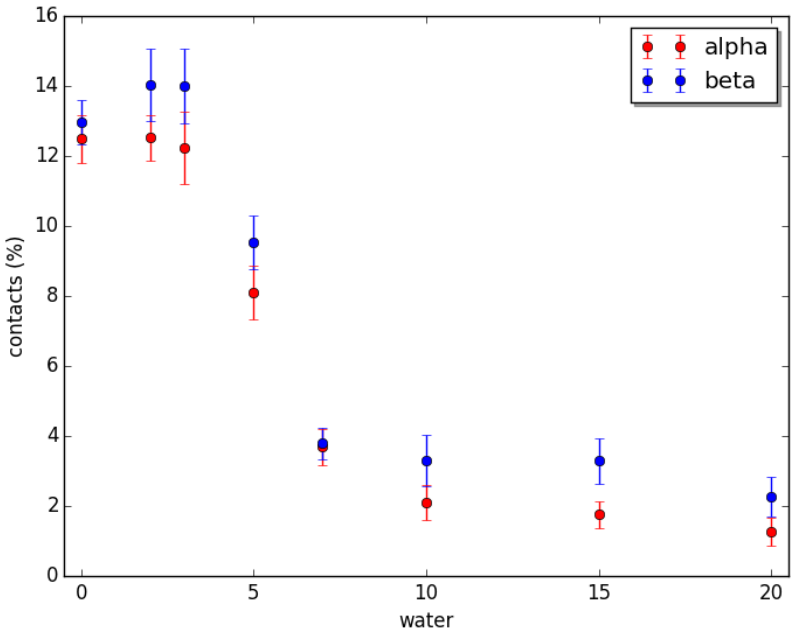

Figure 11

Appendix

Click here to download Appendix: Appendix A.docx